Ocean Engineering 138 (2017) 55–72

Contents lists available at ScienceDirect

Ocean Engineering

journal homepage: www.elsevier.com/locate/oceaneng

A 2D numerical study on suppressing liquid sloshing using a submerged cylinder

A. Iranmanesh, M. Passandideh-Fard*

Department of Mechanical Engineering, Ferdowsi University of Mashhad, Mashhad, Iran

ARTICLE INFO

Keywords:
Free surface flows
Liquid sloshing
Submerged cylinder
Three-step projection method
VOF method

ABSTRACT

In this paper, a two-dimensional numerical model is proposed to study the effect of a submerged cylinder on suppressing liquid sloshing in a moving container. The continuity and Navier-Stokes equations are solved along with an equation for the free surface advection. The Volume of Fluid (VOF) method is used to simulate the free-surface deformation. The numerical model for liquid sloshing is validated with the available experimental, and numerical results in the literature. The results of simulations are in good agreement with those of the measurements. Two scenarios for the liquid sloshing are studied. In the first case, the liquid container is excited with a Constant Acceleration (CA). For the second case, the container is moved with a Single Oscillatory Excitation (SOE). The suppression rate of total kinetic energy of sloshing with the submerged cylinder for two scenarios are calculated and compared to the cases with free sloshing with no cylinder. For the first and second scenarios, using the submerged cylinder reduced the total kinetic energy of sloshing by 26.58% and 71.6%, respectively. Therefore, the effect of submerged cylinder on suppressing the liquid sloshing is more pronounced in the second scenario where the container is excited with the SOE.

1. Introduction

Studying the liquid sloshing of a moving container or externally excited containers are of interest due to their vital role in the transportation of liquids, oil and natural gas (Ibrahim, 2005; Faltinsen and Timokha, 2009). For example, liquid sloshing may generate hydrodynamic forces which can cause structural failure due to undesirable dynamic behaviors.

The sloshing frequencies, mode shapes, and hydrodynamic forces exerted on the rigid walls of a moving cylindrical container under transverse excitation was first studied by Budiansky (1960). Chiba (1995) and Dutta and Laha (2000) showed that the effect of liquid viscosity in reducing the sloshing forces of moving tanks is negligible. Therefore, they proposed baffles to mitigate the sloshing forces to enhance the hydrodynamic damping rate. Several theoretical, experimental, and numerical approaches have been accomplished in the literature to investigate the effects of baffles on the sloshing behavior in liquid containers. Three-dimensional sloshing in a rectangular tank with various fill levels and baffles was evaluated by Akyildiz and Unal (2005) experimentally. The tank was supposed to be excited under pitch oscillations in this study. Pressure distributions were monitored by nine pressure transducers with a special arrangement. They concluded that the sloshing could be diminished significantly by installing horizontal and vertical baffles. Panigrahy (2006) experimentally studied the effect of baffles in suppressing the liquid sloshing, the free surface elevation from the mean static level, and wall pressure of the tanks due to liquid sloshing. Goudarzi and Sabbagh-Yazdi (2012) investigated both analytically and experimentally the effect of three types of baffles namely horizontal and upper- and lower-mounted vertical baffles in suppressing the liquid sloshing. The tank was supposed to be oscillated at the resonant frequency initially. After the steady state condition was reached or the free surface elevation became sufficiently large, the excitation was stopped and the decay rate of free surface oscillation was studied. Akyildiz et al. (2013) experimentally considered the effects of ring baffles on liquid sloshing in a rigid cylindrical tank. The sloshing behavior of the tank was studied under the excitation of roll motion. The rolling frequency varied between 0.83 r/s and 2.0 r/s. Furthermore, three filling depths of 25%, 50%, and 75% were studied in their research. Their experiments were conducted to obtain a practical baffle arrangement which was efficient over a range of rolling frequencies. The hydrodynamic damping of sloshing in circular-cylindrical containers with baffles were investigated by Maleki and Ziyaeifar (2008) experimentally. Their experiment was conducted for water height of 20, 30, 50, 75, and 100 cm with two excitation amplitudes of 0.4 and 1.5 mm. They concluded that the ring baffles were more efficient in suppressing the sloshing oscillations.

* Corresponding author.
E-mail addresses: iranmanesh.aghil@gmail.com (A. Iranmanesh), mpfard@um.ac.ir (M. Passandideh-Fard).

http://dx.doi.org/10.1016/j.oceaneng.2017.04.022
Received 19 November 2016; Received in revised form 10 April 2017; Accepted 17 April 2017

Nomenclature

$\vec{u}$, $\vec{v}$	velocity of the fluid relative to the tank
$\vec{u}^{n+\frac{1}{3}}$,$\vec{u}^{n+\frac{2}{3}}$	intermediate velocity
t	time
ρ	density
p	pressure
μ	dynamic viscosity
$\vec{f}_{B.L}$	external body forces per unit mass for the liquid
$\vec{f}_v$	virtual body force per unit mass
F	volume fraction of a cell occupied by liquid
$\vec{F}$	force
$\dot{\vec{V}}$,a	linear acceleration
$\ddot{\vec{\theta}}$	angular acceleration
$\dot{\vec{\theta}}$,ω	angular velocity
m	mass
I_s	the moment of inertia tensor
$\vec{r}_s$	center of the mass of the solid
$\vec{f}_{B.S}$	force acted on the solid per unit mass due to external body forces
$\vec{R}$	force that is acted on the boundaries of the solid body by the fluid
$\vec{T}$	torque that is acted on the boundaries of the solid body by the fluid
n	outward normal vector to the boundary of volume $\partial\forall$
I_3	3×3 identity matrix
$\vec{u}^*$	velocity of a fluid particle with respect to an inertial reference
$\vec{r}$	position vector of the liquid particle in the moving reference frame
φ_s	volume fraction of solid
K	spring constant
$F_{d,x}$	damper coefficient in x direction
U_s	horizontal velocity of the solid
V_s	vertical velocity of the solid
$\vec{F}^{ST}$	surface tension as a body force term
σ	surface tension
d	water depth
L	length of the container
H	height of the container
H_{P4}	height of point P_4
D_x	diameter of the submerged cylinder in x-direction
D_y	diameter of the submerged cylinder in y-direction
β	spring-damper angle
L_y	vertical projected length of spring-damper
L_x	horizontal projected length of spring-damper
F_d	damping constant
A	amplitude of excitation
f_w	fundamental sloshing frequency
f	excitation frequency
γ	frequency ratio
g	gravity acceleration
$TKE_{ave,free}$	average kinetic energy of free solshing
$TKE_{ave,sub}$	average kinetic energy of solshing with submerged cylinder
Re_{max}	maximum Reynolds number
P_x	power absorbed by dampers in x-direction
E	kinetic energy of each computational cell
We	Weber number

Subscript

s	solid
l	liquid
g	gas

Although experimental results are essential to evaluate the sloshing behavior of moving tanks, attributing these results to the real scale models can be questionable. As a result, theoretical models were also used to analyze the sloshing behavior of tanks with baffles. Hasheminejad and Mohammadi (2011) numerically presented pressure modes of free liquid sloshing in a circular tank with horizontal baffles, bottom-mounted, and surface-piercing vertical baffles. The powerful Laplace transform technique was employed to study the effects of fill ratio and baffle arrangement on the transient sloshing within the partially filled circular containers. They concluded that the surface-piercing vertical baffle was an effective means for mitigating liquid oscillations in higher modes at high fill levels. The sloshing in microgravity condition was tested by Veldman et al. (2007). The test cases were performed in February 2005 in the satellite sloshsat FLEVO while orbiting around the earth. Three orthogonal gyroscopes and six high-quality accelerometers were used to measure the spacecraft motion. Their numerical model was validated with the obtained experimental data. Ebrahimian et al. (2013) suggested a successive boundary element method to model the antisymmetric and symmetric sloshing natural frequencies and mode shapes for the multi-baffled axisymmetric tanks with arbitrary geometries. The Laplace equation and Green's theorem were applied to develop the fluid model. The effects of liquid depth, size and position of the baffle on the sloshing natural frequency were presented. It was reported that the position of the baffle had a more important role on the sloshing natural frequency than the baffle size. Zhang (2015a, 2015b) studied the liquid sloshing in LNG carrier with wedge-shaped tanks using the boundary element method. He investigated the effects of the inclined tank walls on the natural sloshing frequencies and modes. Six inclined angles (α=kπ/24, (k=0,1, ..., 5)) and four fill levels of 10%, 30%, 50%, and 70% were considered in their research. Furthermore, free-surface elevations when the carrier was excited by sway, roll, surge or pitch motions were also studied. It was found that the natural frequencies of diverging containers were more dependent on the variation of the inclined angle in comparison with the converging containers. Zhang (2015a, 2015b) proposed an improved semi-Lagrangian procedure to eliminate the limitation existed on the vertical wall. The approach was used to simulate the nonlinear sloshing waves in non-wall-sided tanks. However, this methodology was only applicable to cases when the body surface was vertical near the waterline. Diverging tanks had angles of π/12, π/6, and π/4 while the angles of converging tanks were -π/12, -π/6, and -π/4. He also investigated 2D and 3D fully nonlinear sloshing waves in wedge-shaped containers. Wang et al. (2016a, 2016b) investigated the effects of the T-shaped baffle on liquid sloshing in horizontal elliptical tanks using a semi-analytical scaled boundary finite-element method. They also considered three T-shaped baffles configurations including surface-piercing and bottom-mounted baffles and their combinations. The effects of baffled arrangement, liquid fill level, and baffle lengths on the sloshing wave height and frequencies were discussed extensively. They concluded that the present approach had the ability to analyze singularity problems and complex sloshing phenomena. Wang et al. (2016a, 2016b) studied the sloshing of stratified liquid with density varying in depth for a three-dimensional cylindrical tank. The governing equation was not Laplacian while the flow of stratified liquid was rotational. They found that the stratification of the liquid density weakened the natural frequencies.

Heikkinen et al. (2013) studied the interaction between waves and cylindrical wave energy converters analytically. They used potential flow theory for both the waves and the oscillating cylinder. It was concluded that the efficiency is highly dependent on the cylinder radius. Wu et al. (2016) studied 3D free-surface potential flows by establishing a mesh-free numerical model. In their scheme, the partial derivatives of velocity potential were precisely calculated, therefore, their model resulted in an accurate prediction of the trajectory of each free-surface node. The model was applied to simulate the free surface waves of sloshing in rectangular, square and cylindrical swaying containers. For 3D liquid sloshing in a square tank, the tank was excited with a slant angle of 30° to the horizontal axis.

A theoretical model was proposed by Isaacson and Premasiri (2001) to evaluate the potential of using baffles to increase the dynamic damping in a rectangular tank undergoing horizontal oscillations. Free liquid sloshing in a rectangular tank with a slat screen mounted vertically in middle of the container was investigated analytically by Faltinsen et al. (2011). The tank was oscillated horizontally while its frequency range covered the two lowest natural sloshing frequencies. Furthermore, they studied the effect of solidity ratio of the baffle on the lateral sloshing.

Viscous sloshing in a rectangular container with harmonic and rolling motion was simulated by Celebi and Akyildiz (2002) using the VOF technique. The Navier-Stokes equations were rewritten because of using a moving coordinate system in their simulation. The fluid was assumed to be Newtonian, viscous, isotropic, and homogenous with a very limited compressibility. The tank was restricted to oscillate along a vertical curve with a rolling motion. The flow regime was laminar while the liquid was supposed to be homogenous. They investigated two filling levels of 7.5 ft and 30 ft in their research. A numerical second-order VOF model was proposed by Liu and Lin (2008) to simulate nonlinear liquid sloshing of a rectangular tank with free surface breakup. The LES scheme was also used to consider the turbulence effects. In another study (Liu and Lin, 2009), they considered the effect of vertical baffles in tanks using virtual boundary force method while the flow regime was supposed to be turbulent. Wu et al. (2012) introduced a time-independent Finite Difference Method (FDM) with fictitious cell technique to investigate liquid sloshing in 2D rectangular tanks with bottom-mounted and surface-piercing baffles. They also studied the effects of baffles on the resonant frequency. The liquid sloshing in a moving partially filled rectangular tank with a vertical baffle was modelled by Akyildiz (2012). The nonlinear behavior of liquid sloshing was simulated using the VOF method. The ratio of baffle height to still water depth varied between 0 and 1.2 while the water depth was supposed to be 75% of the tank height. It was concluded that the liquid sloshing was somewhat suppressed as the baffle height increased, even for small baffles. The sloshing suppression was found to be the results of blockage effects as well as the viscosity of baffle walls.

Xue and Lin (2011) applied a three-dimensional numerical model to investigate viscous liquid sloshing in a tank with internal baffles of various geometries and configurations. The internal baffles with complicated shapes were modelled using virtual boundary force method (VBF). They also investigated liquid sloshing in a 3D prismatic tank with various ring baffle configurations under near-resonant excitations of surge and pitch motions. The dominant response frequencies of the liquid system to external excitations were determined using the Fast Fourier Transform (FFT) technique. They also investigated the behavior of liquid sloshing under six degree-of-freedom (DOF) excitations. They also reported that the ring baffles would reduce the effective natural frequency of the liquid system in the tank. Xue et al. (2013) conducted some experiments on a liquid sloshing experimental rig to investigate liquid sloshing phenomenon in a rectangular tank with perforated baffles. They tried to estimate the free surface fluctuation and pressure distribution by changing external excitation frequency. They also used an in-house code to simulate the three-dimensional liquid sloshing in a rectangular tank with perforated baffles. The free surface elevation and pressure distribution calculated by numerical approach were in good agreement with those obtained experimentally. They also applied the Fast Fourier Transform (FFT) technique to achieve spectral analysis of the time history of free surface elevation. They concluded that the damping effects of perforated baffles would be more pronounced as the external excitation frequency was increased.

Koh et al. (2013) improved Consistent Particle Method (CPM) to omit pressure fluctuation. They utilized the improved CPM (so called the CPM-5 method) to model water sloshing with a constrained floating baffle (CFB) numerically while the flow regime was supposed to be laminar. They also investigated the effect of the CFB in suppressing the water sloshing. The experimental data were used to verify the numerical model. Li et al. (2014a, 2014b) developed the Material Point Method (MPM) to predict the dynamic behavior of liquid sloshing in a moving rectangular tank. A special approach was presented to apply harmonic excitation to the container while the filling level of water was supposed to be 15% of the total height of the container. Furthermore, the frequency of external excitation was supposed to be constant in all cases(0.4255 Hz). They verified the MPM scheme in modelling liquid impact pressure by comparing the numerical results with a water block dropping test onto an aluminum plate. They concluded that the MPM model well predicted the slosh-induced impact pressures on the vertical walls of the tank in comparison with the experimental data. Li et al. (2014a, 2014b) developed a parallel code to model water movement in rectangular tanks under rolling and horizontal excitations using the VOF method. They also measured the pressure on the tank walls which compared well with those of simulations. Furthermore, they conducted studies based on various fill levels and excitation frequencies. They found that the tree-based adaptive VOF method is capable of simulating the sloshing problems with low water depth and severe non-linearity. Elahi et al. (2015) developed a two-dimensional numerical model to investigate the behavior of liquid sloshing in rectangular containers including liquid viscosity and surface tension. The free-surface deformation was also modelled by the VOF method and the flow regime was supposed to be laminar. Their model was applied to study the sloshing of a liquid tank where the container had both linear and rotational accelerations. Zhang et al. (2015) applied the 3D Boundary Element Method (BEM) to study the second-order resonance problems in rectangular sloshing containers undergoing a harmonic excitation. They reported that the interaction among excitation frequencies and natural frequencies may generate the second-order resonance. They also concluded that the second-order resonance emerged much earlier as the excitation amplitude increased. Luo et al. (2016) developed a three-dimensional Consistent Particle Method (CPM) to study violent sloshing under regular and irregular excitations. The frequency varied between 0.2 and 2.0 rad/s with an increment of 0.02 rad/s. They reported that the stability of ship motion was mostly influenced by the sloshing waves in the beam sea sailing condition. Hwang et al. (2016) utilized a modified particle-based Fluid-Structure Interaction (FSI) solver to model sloshing flows in rolling rectangular containers with elastic baffles. They assumed that the period of rolling motion was 85% of natural period of the tank while the rolling amplitude was 4°. They compared the results of the sloshing for various cases without any baffle, with a rigid baffle and a set of flexible baffles. Cavalagli et al. (2017) accomplished an experimental-numerical study on sloshing phenomenon in moving tuned sloshing dampers. An electric torsional servomotor coupled with a ball screw transmission device was used to generate the harmonic displacement. They studied the sloshing behavior of a rectangular rank for various amplitudes, frequencies, and depths of the inner liquid both experimentally and numerically. It was concluded that the computational fluid dynamic model was able to present an accurate estimation of the dissipated energy in various conditions.

Anbarsooz et al. (2014) predicted the behavior of the submerged circular cylinder Wave Energy Converter (WEC) subjected to highly nonlinear incident waves by solving the complete solution of the Navier-Stokes equations. They found that the numerical wave tank is capable of predicting the wave-body interactions as long as the flow regime is laminar. Malvandi et al. (2016) solved two-dimensional Navier-Stokes equations on a regular structured grid to simulate different scenarios: a cylinder falling into a rectangular domain due to gravity; transient vertical oscillation of a cylinder released above its equilibrium position; and a dam breaking in presence of a fixed obstacle. The flow regime was supposed to be laminar in their research. The fluid free surface and the solid object was modelled using the level set and the immersed boundary methods, respectively. The developed code was also applied to simulate the interaction of a buoy in a water wave tank with symmetrical and asymmetrical waves. Iranmanesh and Passandideh-Fard (2017) applied a three-dimensional numerical scheme to simulate the water entry of a horizontal circular cylinder using the VOF method. The continuity and Navier-Stokes equations were solved everywhere in the computational domain including the solid object. They also studied the effects of cylinder diameter, length, impact velocity, and cylinder-water density ratio on the non-dimensional depth. It was concluded that three-dimensional effects could be neglected for cylinder lengths larger than 0.2 m.

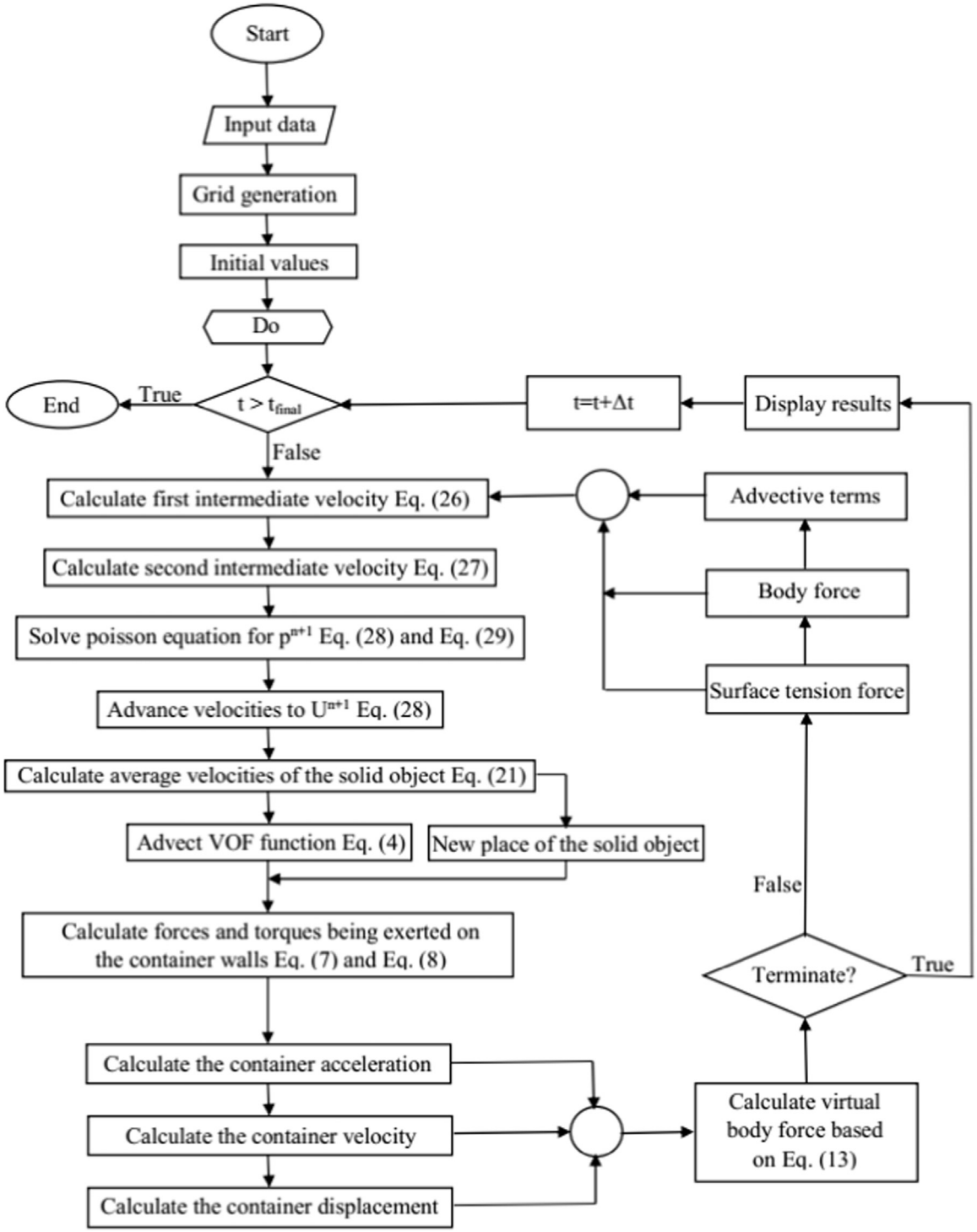

Fig. 1. Flowchart of the numerical model developed to simulate the sloshing of a moving container in presence of a submerged object.

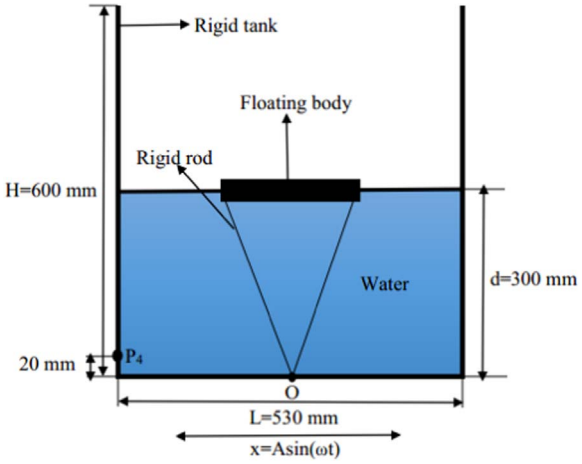

Fig. 2. Schematic diagram of water sloshing with the CFB.

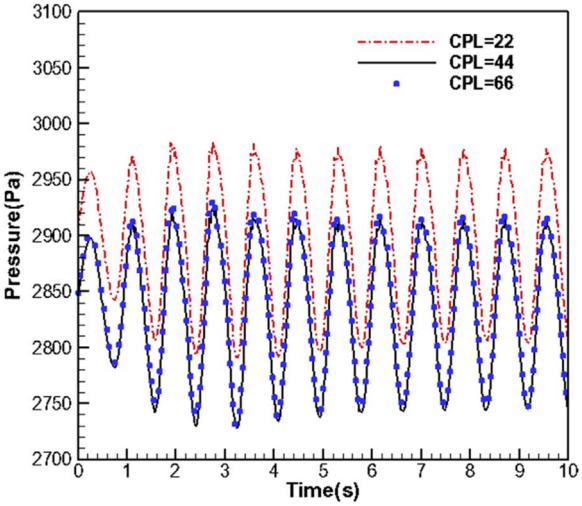

Fig. 3. The results of mesh refinement study for the pressure at point P_4 versus time.

Studying the effect of a submerged cylinder in reducing the kinetic energy of sloshing waves under various excitations in the literature is rare. Therefore, the feasibility of using a submerged cylinder as a mitigation device to absorb the kinetic energy of water sloshing is numerically studied in this paper. Two scenarios with a Constant Acceleration (CA) and Single Oscillatory Excitation (SOE) are considered. To validate the numerical model, the results are compared with numerical and experimental results available in the literature. To confirm that the submerged cylinder can mitigate the sloshing kinetic energy, excitation amplitude and frequency, water depth, cylinder diameter, density, and position will be varied and the effects of the submerged cylinder in mitigating the sloshing kinetic energy will be studied separately.

2. Mathematical model

2.1. Fluid dynamics

It is necessary to simulate the motion of the fluid in presence of the solid-body movement for sloshing phenomenon. Therefore, earth-fixed and body-fixed coordinate systems are defined for this purpose to facilitate the simulation process. The unsteady, incompressible, continuity and Navier-Stokes equations in two-dimensional and laminar form are:

$$\nabla . \vec{u} = 0 \tag{1}$$

$$\frac{\partial \vec{u}}{\partial t} + (\vec{u} . \nabla)\vec{u} = -\frac{1}{\rho}(\nabla p - \mu(\nabla . \nabla)\vec{u}) + \overrightarrow{f_{B.L}} + \vec{f_v} \tag{2}$$

where $\vec{u}$ stands for the fluid velocity relative to the tank, ρ density, μ dynamic viscosity, p pressure, and $\overrightarrow{f_{B.L}}$ denotes the external body forces per unit mass for the liquid. By applying the Continuum Surface Force (CSF) scheme, $\overrightarrow{f_{B.L}}$ also models the surface tension effects acting on the interfacial cells. $\vec{f_v}$ represents the virtual body force per unit mass resulting from the effects of the container motions on the liquid momentum into the Navier-Stokes equations. The VOF method is used to advect the interface by defining a scalar field F that denotes the volume fraction of a cell occupied by liquid. This function, therefore, is defined as follows:

$$\begin{cases} \text{If } F = 0 & \text{in gas} \\ \text{If } 0 < F < 1 & \text{in liquid–gas interface} \\ \text{If } F = 1 & \text{in liquid} \end{cases} \tag{3}$$

$$\frac{\partial F}{\partial t} + \vec{u} . \vec{\nabla} F = 0 \tag{4}$$

Eq. (4) is solved based on the Youngs PLIC algorithm to track the liquid-gas interface (Youngs, 1984).

2.2. Solid body dynamics

To simulate the solid-body motion, both linear and angular momentum equations should be solved:

$$m_s \vec{\dot{V}} + \vec{\ddot{\theta}} \times m_s \vec{r}_s + \vec{\dot{\theta}} \times (\vec{\dot{\theta}} \times m_s \vec{r}_s) = \vec{R} + m_s \vec{f}_{B.S} \tag{5}$$

$$m_s \vec{r}_s \times \vec{\dot{V}} + I_s \vec{\ddot{\theta}} + \vec{\dot{\theta}} \times (I_s \vec{\dot{\theta}}) = \vec{T} + m_s \vec{r}_s \times \vec{f}_{B.S} \tag{6}$$

These equations are in earth-fixed coordinate system and linear and angular accelerations ($\vec{\dot{V}}$ and $\vec{\ddot{\theta}}$) are unknown in the above equations. m_s denotes the mass of solid body, I_s the moment of inertia tensor, and $\vec{r}_s$ represents the center of the solid mass. The force acted on the solid per unit mass due to external body forces is shown by $\vec{f}_{B.S}$. The force and torque acted on the boundaries of the solid body by the fluid via pressure and viscous effects are shown by $\vec{R}$ and $\vec{T}$, respectively:

$$\vec{R} = \oint_{\partial \forall} (pI_3 - \mu \nabla \vec{u}) . nds \tag{7}$$

$$\vec{T} = \oint_{\partial \forall} (\vec{r} \times (pI_3 - \mu \nabla \vec{u})) . nds \tag{8}$$

where n is the outward normal vector to the boundary of volume ∂∀ and I_3 stands for the 3×3 identity matrix. After calculating linear and angular accelerations from Eqs. (5) and (6), velocity and displacement of the container can be easily determined.

2.3. Virtual body force method

The velocity of a fluid particle with respect to an earth-fixed coordinate system is defined by $\vec{u}^*$ while $\vec{u}$ stands for the velocity of the same particle with respect to the body-fixed coordinate system (*x*-direction). The following relation exists between $\vec{u}^*$ and $\vec{u}$:

$$\frac{D\vec{u}^*}{Dt} = \vec{\dot{V}} + \vec{\ddot{\theta}} \times \vec{r} + \vec{\dot{\theta}} \times (\vec{\dot{\theta}} \times \vec{r}) + \frac{D\vec{u}}{Dt} + 2\vec{\dot{\theta}} \times \vec{u} \tag{9}$$

$$\vec{\dot{V}} = \left(\frac{d\vec{V}}{dt}\right) + \vec{\dot{\theta}} \times \vec{V} \tag{10}$$

where $\vec{\ddot{\theta}}$, $\vec{\dot{\theta}}$, $\vec{r}$ are the angular acceleration, angular velocity and the position vector of the liquid particle in the moving reference frame,

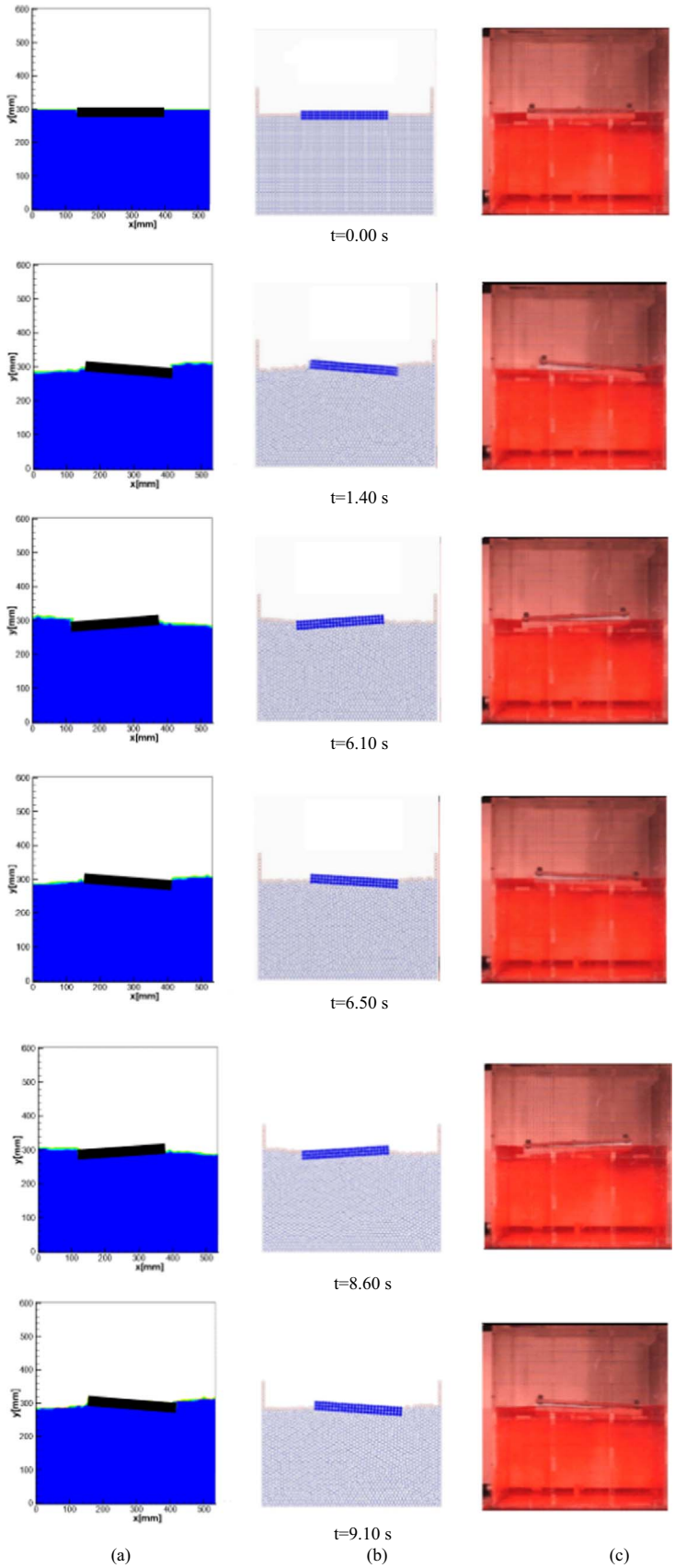

Fig. 4. Water sloshing with constrained floating baffle (a) Present study (b) Available numerical results using the CPM-5 method (Koh et al., 2013) (c) Experiment (Koh et al., 2013).

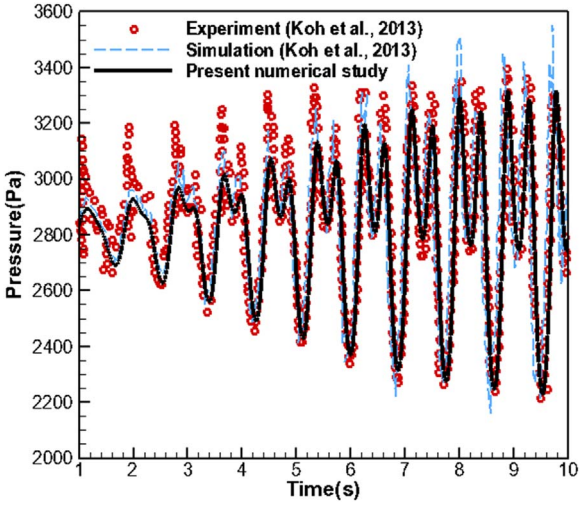

Fig. 5. Pressure history of free sloshing in a rectangular tank at point P_4.

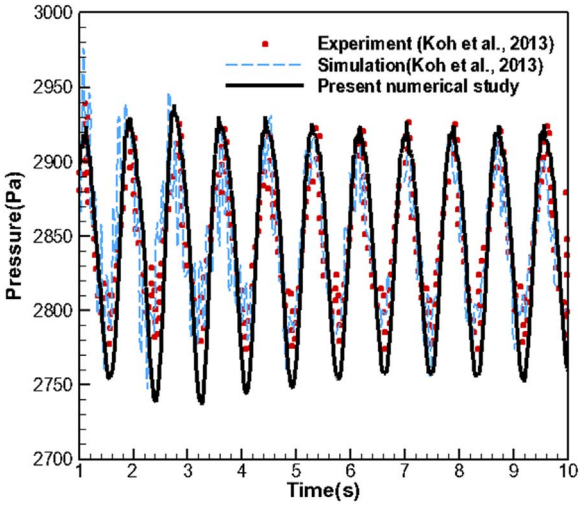

Fig. 6. Pressure history of sloshing with the CFB in a rectangular tank at point P_4.

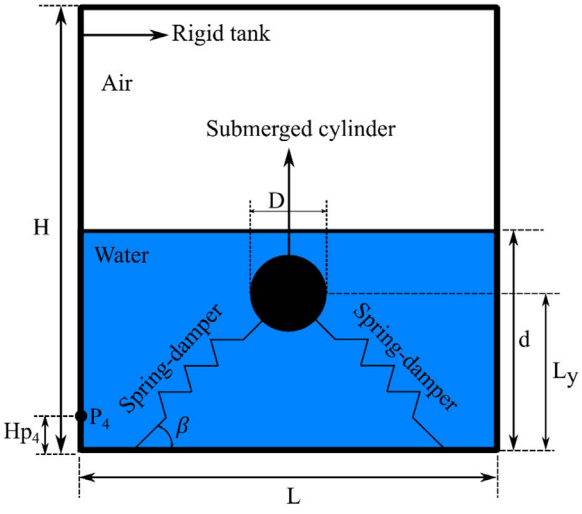

Fig. 7. Schematic diagram of a container equipped with the submerged cylinder.

respectively. $\vec{\dot{V}}$ denotes the acceleration of the moving origin with respect to the origin of the inertial reference frame. The centrifugal and Coriolis accelerations are also represented by the third and fifth terms in the right-hand side of Eq. (9). It should be noted that the velocity in the body-fixed coordinate system ($\vec{u}$) is related to the velocity in the earth-fixed coordinate system ($\vec{u^*}$) by using Eq. (9) and this equation is only used to eliminate ($\vec{u^*}$) in Eq. (11). Now, the Navier-Stokes equations are:

$$\frac{D\vec{u^*}}{Dt} = -\frac{1}{\rho}(\nabla p - \mu(\nabla.\nabla)\vec{u}) + \vec{f_{B.L}} \tag{11}$$

Combining Eqs. (9) and (11) results in:

$$\frac{D\vec{u}}{Dt} = -\frac{1}{\rho}(\nabla p - \mu(\nabla.\nabla)\vec{u}) + \vec{f_{B.L}} + \vec{f_v} \tag{12}$$

where $\vec{f_v}$ is:

$$\vec{f_v} = -\vec{\dot{V}} - \vec{\ddot{\theta}} \times \vec{r} - \vec{\dot{\theta}} \times (\vec{\dot{\theta}} \times \vec{r}) - 2\vec{\dot{\theta}} \times \vec{u} \tag{13}$$

Small changes are required for the liquid dynamics since Eq. (12) is completely similar to Eq. (2). $\vec{f_v}$ in Eq. (12) can be interpreted as acceleration due to a virtual body force based on the Newtons's third law. In other words, an acceleration equal in magnitude and opposite in sign is applied on the fluid instead of actually moving the solid body in the numerical model.

By using Eq. (12) and the divergence theorem, Eqs. (7) and (8) are simplified to:

$$\vec{R} = \oint_{\forall} (\nabla p - \mu(\nabla.\nabla)\vec{u}) d\forall = -\oint_{\forall} \rho\left(\frac{D\vec{u}}{Dt} - \vec{f_{B.L}} - \vec{f_v}\right) d\forall \tag{14}$$

$$\vec{T} = \oint_{\forall} (\vec{r} \times (\nabla p - \mu(\nabla.\nabla)\vec{u})) d\forall = -\oint_{\forall} \left(\rho\vec{r} \times \left(\frac{D\vec{u}}{Dt} - \vec{f_{B.L}} - \vec{f_v}\right)\right) d\forall \tag{15}$$

2.4. Numerical stability of the dynamic model

If Eqs. (5) and (6) are integrated directly with respect to time, the result of integration will not be stable for all arbitrary liquid/mass ratios. A new coupling scheme was proposed by Veldman et al. (2007) to resolve this challenge. The new methodology is derived as follows:

$$m\vec{\dot{V}} + \vec{\ddot{\theta}} \times m\vec{\bar{r}} + \vec{\dot{\theta}} \times (\vec{\dot{\theta}} \times m\vec{\bar{r}}) = \oint_{\forall} \rho\left(\frac{D\vec{u}}{Dt} + 2\vec{\dot{\theta}} \times \vec{u} - \vec{f_{B.L}}\right) d\forall + m_s\vec{f_{B.S}} \tag{16}$$

$$m\vec{\bar{r}} \times \vec{\dot{V}} + I\vec{\ddot{\theta}} + \vec{\dot{\theta}} \times (I\vec{\dot{\theta}}) = \oint_{\forall} \left(\rho\vec{r} \times \left(\frac{D\vec{u}}{Dt} + 2\vec{\dot{\theta}} \times \vec{u} - \vec{f_{B.L}}\right)\right) d\forall + m_s\vec{\bar{r}} \times \vec{f_{B.S}} \tag{17}$$

where $m=m_s+m_l$ and $I=I_s+I_l$. The center mass of the coupled method is calculated using the following equation (Elahi et al., 2015):

$$r = \frac{m_s\bar{r}_s + m_l\bar{r}_l}{m} \tag{18}$$

2.5. Solid object modelling

The submerged circular cylinder is modelled using the fast-fictitious-domain method to absorb the sloshing kinetic energy. In this method, the fluid flow equations are applied everywhere considering fluid and solid zones (Mirzaii and Passandideh-fard, 2012). This methodology will result in a considerable reduction of time for computation because of the discretization by a structured and fixed grid mesh and time independent of the computational zone. Glowinski et al., (1999, 2001), Patankar (2001), Patankar et al. (2000) and Sharma and Patankar (2005) developed numerical schemes based on

Table 1
The amount of input parameters used to simulate the liquid sloshing of container with a submerged cylinder (CA).

d (m)	L (m)	H (m)	D (m)	β (deg)	L_y (m)	K (N/m)	F_d (N)
0.0625	0.25	0.25	0.025	45	0.04	960	6.0
ρ_l(kg/m^3)	ρ_s(kg/m^3)	ρ_g(kg/m^3)	μ_l(kg/ms)	μ_s(kg/ms)	μ_g(kg/ms)	H_{P4}(m)	ω_s(rad/s)
998.2	1000	1.225	0.001003	0.1003	1.789e−5	0.02	0

the fast-fictitious-domain method. A modified version of Sharma and Patankar (2005) scheme presented by Mirzaii and Passandideh-fard (2012) is used in this research to treat the solid object. The advantage of this method is that no additional equation in the computational zone is required. The viscosity within the solid zone is increased to apply the no-slip condition on the liquid-solid interface. The governing equations of fluid motion are imposed initially everywhere within the computational domain considering the liquid and solid zones. The rigid body motion for the submerged cylinder can be achieved by conserving the total linear and angular momentums within the solid zone in each time step. Sharma and Patankar (2005) stated that applying an average velocity for the solid zone would result in an unrealistic slip condition in the solid-liquid interface. To resolve this difficulty, the viscosity of the solid zone is increased in this research. The computational procedures achieved in each time step are listed below briefly:

1. By defining a scalar parameter φ_s, the solid object in the computational domain is designated

$$\begin{cases} \text{If } \varphi_s = 0 & \text{out of the solid body} \\ \text{If } 0 < \varphi_s < 1 & \text{solid interface} \\ \text{If } \varphi_s = 1 & \text{in solid} \end{cases}$$

2. As stated, the fluid flow equations are imposed everywhere within the computational domain. The following relations are used to calculate the density and viscosity in each cell

$$\rho = F\rho_l + (1 - F - \varphi_s)\rho_g + \varphi_s\rho_s \tag{19}$$

$$\mu = F\mu_l + (1 - F - \varphi_s)\mu_g + \varphi_s\mu_s \tag{20}$$

where liquid, gas and solid are represented by l, g and s respectively. Mirzaii and Passandideh-Fard (2012) stated that a solid viscosity two orders of magnitude larger than that of the fluid was adequate to remove the effects of an unrealistic slip emerging in the solid-liquid interface. It is also supposed that volume fraction (F) within the solid zone is set to zero.

3. The average rotational and translational velocities for the submerged cylinder are calculated by conserving total momentum within the solid zone

$$m_s \vec{U_s} = \int_{Solid\ zone} \rho \vec{u}\ d\forall \tag{21}$$

$$I_s \vec{\omega_s} = \int_{Solid\ zone} \vec{r} \times \rho \vec{u}\ d\forall \tag{22}$$

After replacing the solid velocity with the above average velocities, the interface is advected using Eq. (4).

2.6. Numerical Implementation of springs and dampers

To apply the effects of springs and dampers on the rigid motion of the submerged cylinder, a body force term is added only to momentum equations solved for the solid zone. The following relation is used to calculate the spring and damper body force terms per unit mass:

$$\vec{a}_{added} = \frac{\sum \vec{F}_{external}}{m_s} \tag{23}$$

This equation should be calculated in x and y directions. Therefore, we have:

$$a_{x,added} = \frac{\sum F_{x,external}}{m_s} = \frac{-k_{sx}(x_{c,s} - x_{free}) - (F_d)_x}{m_s} \tag{24}$$

$$a_{y,added} = \frac{\sum F_{y,external}}{m_s} = \frac{-k_{sy}(y_{c,s} - y_{free}) - (F_d)_y}{m_s} \tag{25}$$

Spring constants and damper coefficients in x and y directions are denoted by $k_{s,x}$, $k_{s,y}$, $(F_d)_x$, $(F_d)_y$ respectively. x_{free} and y_{free} are the free lengths of springs in x and y directions while the center positions of the submerged cylinder are shown by $x_{c,s}$ and $y_{c,s}$, respectively.

A three-step projection method is used to discretize the momentum and continuity equations in three fractional steps (Mirzaii and Passandideh-Fard, 2012). An explicit scheme is used to consider the convective and body force terms in the first step. So, an intermediate velocity ($\vec{u}^{n+\frac{1}{3}}$) is calculated as follows:

$$\frac{\vec{u}^{n+\frac{1}{3}} - \vec{u}^{n}}{\Delta t} = -(\vec{u} \cdot \nabla \vec{u})^n + \frac{1}{\rho^n} \overrightarrow{f_{B.L}}^{\,n} \tag{26}$$

Using an explicit approach for discretizing the viscous term in the momentum equations will result in decreasing the time step due to the constraint on stability of an explicit method (Harlow and Amsden, 1971). So, an implicit scheme is applied to calculate the intermediate velocity ($\vec{u}^{n+\frac{2}{3}}$) in the second step to eliminate the time step restriction of viscous term:

$$\frac{\vec{u}^{n+\frac{2}{3}} - \vec{u}^{n+\frac{1}{3}}}{\Delta t} = \frac{1}{\rho^n} \nabla \cdot \mu[(\nabla \vec{u}^{n+\frac{2}{3}}) - (\nabla \vec{u}^{n+\frac{2}{3}})^T] \tag{27}$$

A Tri-Diagonal Matrix Algorithm (TDMA) method is used to solve Eq. (27) in the fractional step $t^{n+\frac{2}{3}}$. As the final step, the second intermediate velocity is applied to obtain the velocity at the next time level (n+1) using an implicit method:

$$\frac{\vec{u}^{n+1} - \vec{u}^{n+\frac{2}{3}}}{\Delta t} = -\frac{1}{\rho^n} \nabla \cdot p^{n+1} \tag{28}$$

Writing the continuity equation for the new time level will lead to:

$$\nabla \cdot \vec{u}^{n+1} = 0 \tag{29}$$

Taking divergence of Eq. (28), and combining it with Eq. (29) will result in:

$$\nabla \cdot \left[\frac{1}{\rho^n} \nabla p^{n+1}\right] = \frac{\nabla \cdot \vec{u}^{n+\frac{2}{3}}}{\Delta t} \tag{30}$$

Pressure can be calculated from Eq. (30) using Incomplete Cholesky-Conjugate Gradient (LDL) solver (Kershaw, 1978). Velocity at the new time level can be estimated by substituting the calculated pressure into Eq. (28).

The surface tension term in the momentum equation is modelled as a body force using the Continuum Surface Force (CSF) by Brackbill et al. (1992). The following relation was proposed for $\vec{F}^{ST}$ by Aleinov and Puckett (1995):

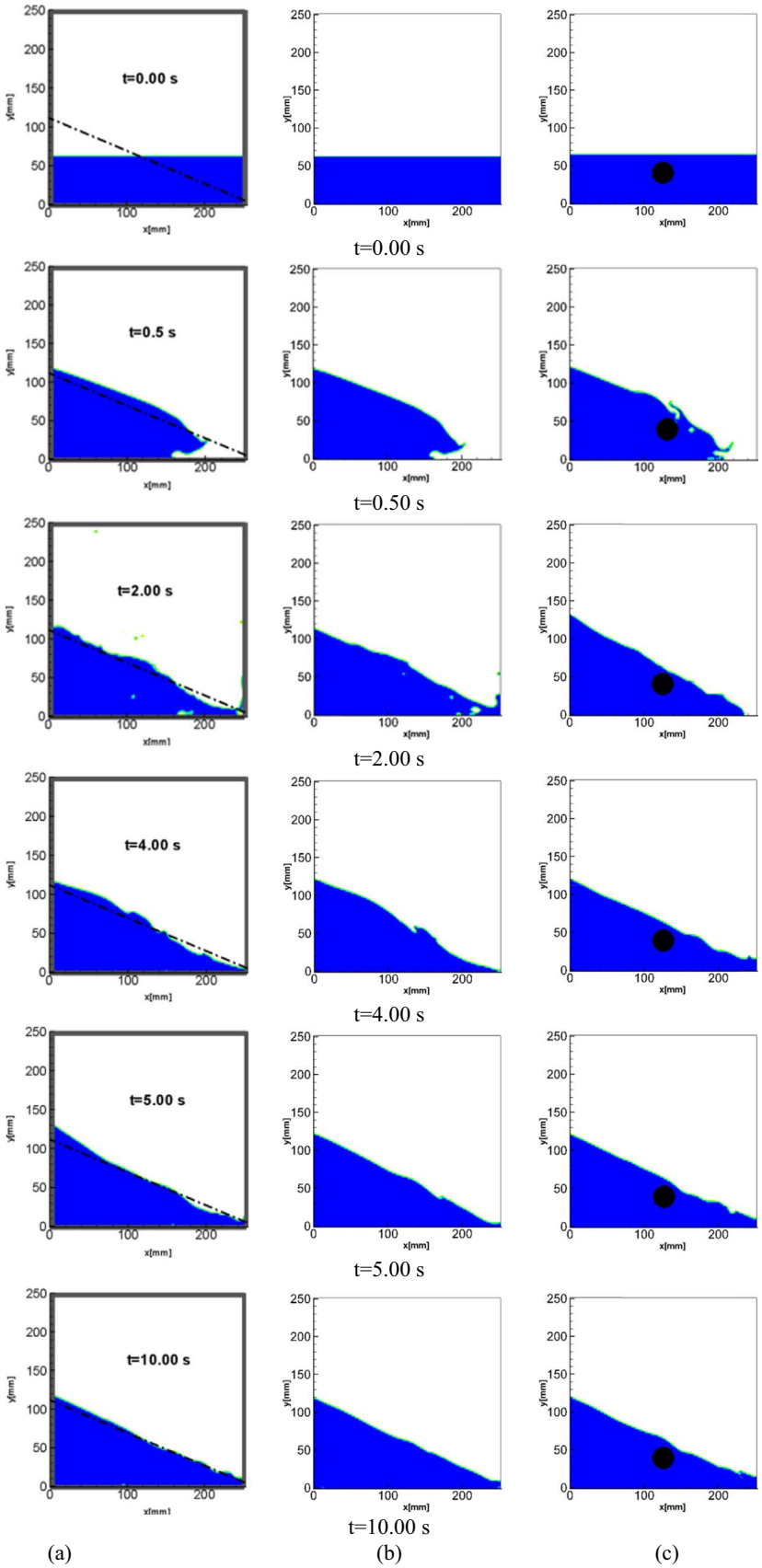

Fig. 8. Liquid sloshing of a moving container under an excitation (CA) (a) Analytical and numerical results (Elahi et al., 2015), (b) Present study (Free sloshing), and (c) Present study (Sloshing with the submerged cylinder).

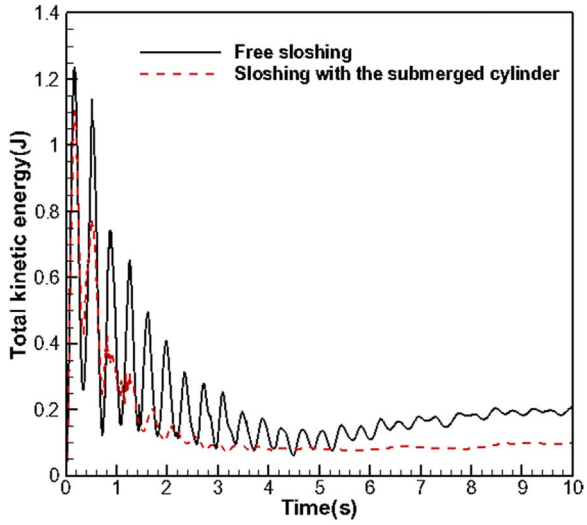

Fig. 9. Total kinetic energy of the sloshing with and without the submerged cylinder versus time (CA).

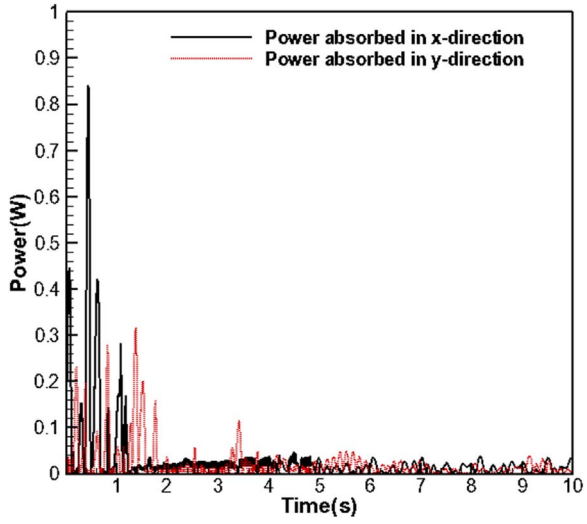

Fig. 10. Power absorbed by the damper in x and y directions versus time for the case of sloshing with the submerged cylinder (CA).

Table 2
Effect of the submerged cylinder on suppressing the kinetic energy of the liquid sloshing undergoing the CA.

$U_{s,max}$ (m/s)	Re_{max}	$TKE_{ave,free}$ (J)	$TKE_{ave,sub}$ (J)	Rate of suppression (%)
0.1948	4846.69	0.2671	0.1961	26.58

$$\overrightarrow{F}^{ST} = \sigma\kappa\frac{A}{V}\hat{n} \tag{31}$$

where σ, A, V are surface tension, the surface area of the fluid contained within the cell and cell volume respectively. κ and $\hat{n}$ can also be estimated based on the following relations:

$$\kappa = -\nabla.\ \hat{n} \tag{32}$$

$$\hat{n} = \frac{\nabla F}{|\nabla F|} \tag{33}$$

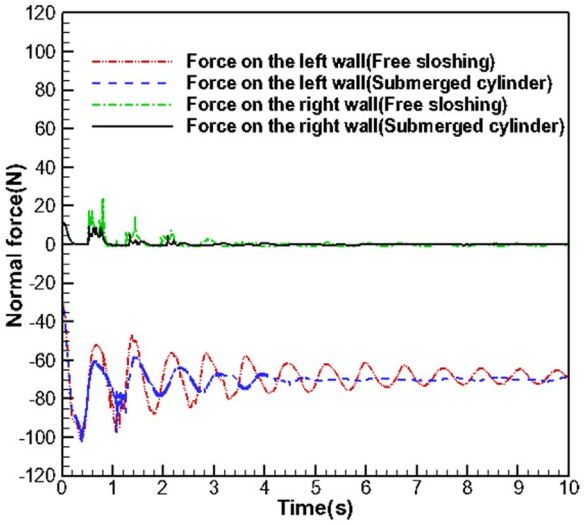

Fig. 11. The amount of normal forces exerted on the left and right walls subjected to the free sloshing and sloshing with the submerged cylinder (CA).

The flowchart of the numerical model developed in this paper is illustrated in Fig. 1.

3. Results and discussion

3.1. Mesh refinement study and validation

The schematic diagram of the moving container is shown in Fig. 2. All the input data used in the simulations are those of the experiments performed by Koh et al. (2013). The excitation amplitude and the frequency of the moving container are 0.004 m and ω=7.3996 rad/s, respectively. The length and height of the container, and the water depth are denoted by L, H, and d, respectively. The amount of these parameters are also represented in Fig. 2. For the case with baffles, the density amount of the Constrained Floating Baffle (CFB) is 520 kg/m^3 which is assumed to be smaller than that of water. The length and thickness of the floating baffle are also set to be 0.26 m and 0.03 m, respectively. The floating body is constrained by rigid rods hinged to the bottom of the container at point O. A pressure sensor in the experiment (Koh et al., 2013) was positioned at point P_4 to measure the pressure. The number of cells per length (CPL) of the CFB is defined to examine the mesh refinement study. The cell size was progressively decreased until no significant changes in the results for the pressure at point P_4 were observed. The results of this study versus time are shown in Fig. 3. Based on this figure, the amount of CPL is finally set to 44 to simulate the liquid sloshing with the CFB.

To validate the developed numerical code both quantitatively and qualitatively, the present numerical results are compared with the available experimental and numerical results in the literature for two cases. The results of liquid sloshing within a moving container without any baffle are first examined. Next, a solid object considered as the CFB is implemented to the numerical code to suppress violent sloshing waves. The results of water sloshing with the CFB at six time instants are compared qualitatively with those reported in the literature (Koh et al., 2013) in Fig. 4. A good agreement is observed between the results of simulations with both numerical and experimental results of Koh et al. (2013). As observed, the CFB does not allow the liquid to move as a standing wave and it mitigates the sloshing effectively with no wave breaking within the fluid.

For a quantitative comparison of the simulation results, the pressure history of free sloshing and sloshing with the CFB at a set point (P_4 in Fig. 2) obtained from the present model are compared with the experimental and numerical results (using the CPM-5 method) of

Table 3
The amount of input parameters used to simulate the liquid sloshing of container with a submerged cylinder undergoing the SOE (d4A15).

d (m)	L (m)	H (m)	D (m)	β (deg)	L_y (m)	K (N/m)	F_d (N)	ω_s (rad/s)
0.04	0.4	0.25	0.025	45	0.02	960	6.0	0
ρ_l(kg/m^3)	ρ_s(kg/m^3)	ρ_g(kg/m^3)	μ_l(kg/ms)	μ_s(kg/ms)	μ_g(kg/ms)	A (m)	γ	H_{P4}(m)
998.2	1000	1.225	0.001003	0.1003	1.789e−5	0.015	1	0.02

Table 4
The amount of input parameters used to simulate the liquid sloshing of container with a submerged cylinder undergoing the SOE (d6A10).

d (m)	L (m)	H (m)	D (m)	β (deg)	L_y (m)	K (N/m)	F_d (N)
0.06	0.4	0.25	0.035	45	0.04	960	6.0
ρ_l(kg/m^3)	ρ_s(kg/m^3)	ρ_g(kg/m^3)	μ_l(kg/ms)	μ_s(kg/ms)	μ_g(kg/ms)	A (m)	γ
998.2	1000	1.225	0.001003	0.1003	1.789e−5	0.010	1

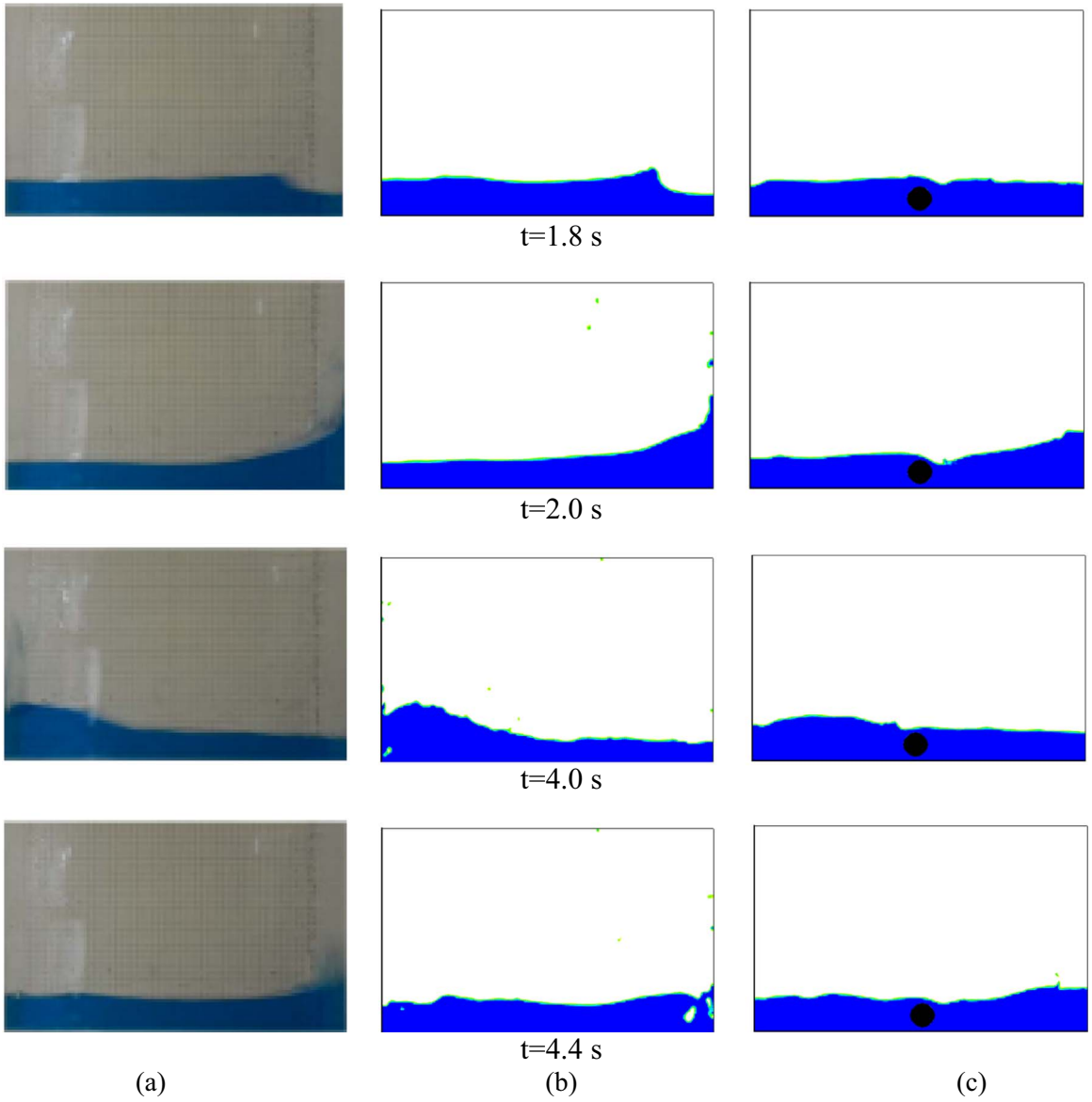

Fig. 12. Liquid sloshing of a moving container undergoing the SOE in x-direction: (a) Experiment (Cavalagli et al., 2017), (b) Present study (without the submerged cylinder), (c) Present study (with the submerged cylinder) (d4A15).

Koh et al. (2013) in Figs. 5 and 6 respectively. For the case of free sloshing without any baffle (Fig. 5), both the CPM-5 and present numerical scheme cannot predict the pressure at point P4 during the transient condition (before t=5 s) with a good accuracy. However, the difference between the numerical results (CPM-5 and present study) and measurements decreases as the system approaches the steady-state condition. The difference may be attributed to the transient characteristics of excitation at the beginning of the experiment. As observed in

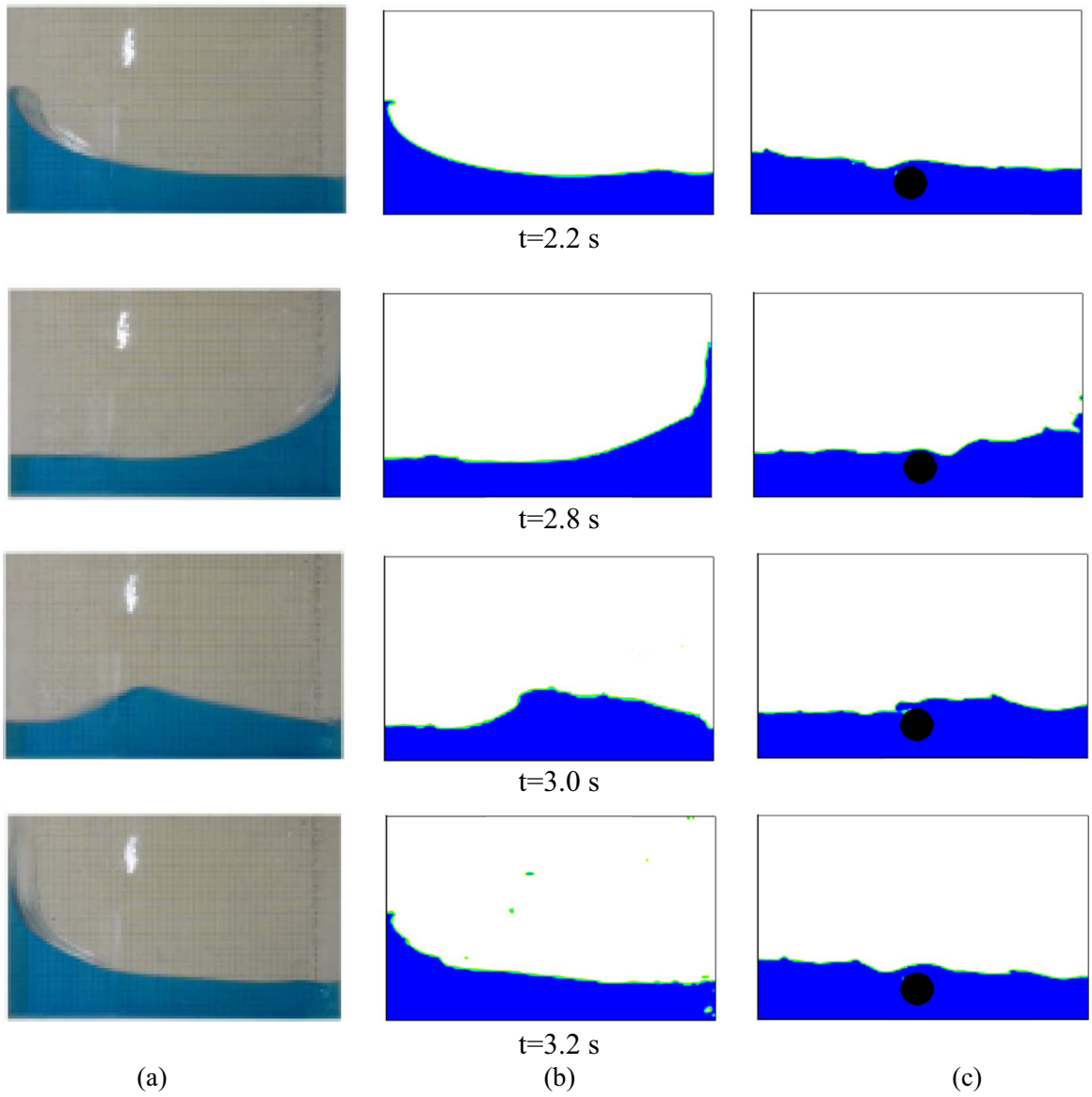

Fig. 13. Liquid sloshing of a moving container undergoing the SOE in x-direction: (a) Experiment (Cavalagli et al., 2017), (b) Present study (without the submerged cylinder), (c) Present study (with the submerged cylinder) (d6A10).

Figs. 5 and 6, at later times, the results of simulations from both the CPM-5 method and the developed model in this study, agree well with those of the experiments in terms of both the pressure amplitude and frequency.

3.2. Suppressing the kinetic energy of liquid sloshing under an excitation with the CA

In this part, the feasibility of using a submerged cylinder as a mitigation device to decrease the kinetic energy of liquid sloshing under an excitation with the CA is investigated. The schematic diagram of the container with a submerged cylinder is presented in Fig. 7.

D stands for the diameter of the submerged cylinder while the vertical projected length in y direction and angle of the spring-damper are shown by L_y and β, respectively. The spring and damping constants are represented by K and F_d. It should be noted that the frictional damper and spring constants are measured experimentally by means of ZWICK Z250 testing machine at Ferdowsi University of Mashhad. The amount of above parameters used for the simulations in this study are given in Table 1.

It is assumed that the container starts to move in x-direction with a constant acceleration of 4.5 m/s^2. Furthermore, it is supposed that the amount of water in case of free sloshing is exactly equal with that of sloshing with the submerged cylinder. Therefore, the effect of the submerged cylinder on reducing the kinetic energy can be studied exclusively while the other conditions are completely the same. It should be mentioned that the values presented for water depth(d) are for the case of free sloshing.

Fig. 8 illustrates the effect of the submerged cylinder on liquid sloshing qualitatively. In this figure, the sloshing of the moving container with and without the submerged cylinder for the first ten seconds are compared with the analytical and numerical results in the literature. As shown in Fig. 8, the slope of the liquid free surface for the case of free sloshing agrees well with the analytical and numerical data presented by Elahi et al. (2015). It should be mentioned that the submerged cylinder cannot change the free surface slope when the container undergoes the CA.

The kinetic energy (E) of the cells occupied by the liquid can be calculated as follows:

$$E = \frac{1}{2} \times m_l \times (|\vec{u}|^2 + |\vec{v}|^2) \tag{34}$$

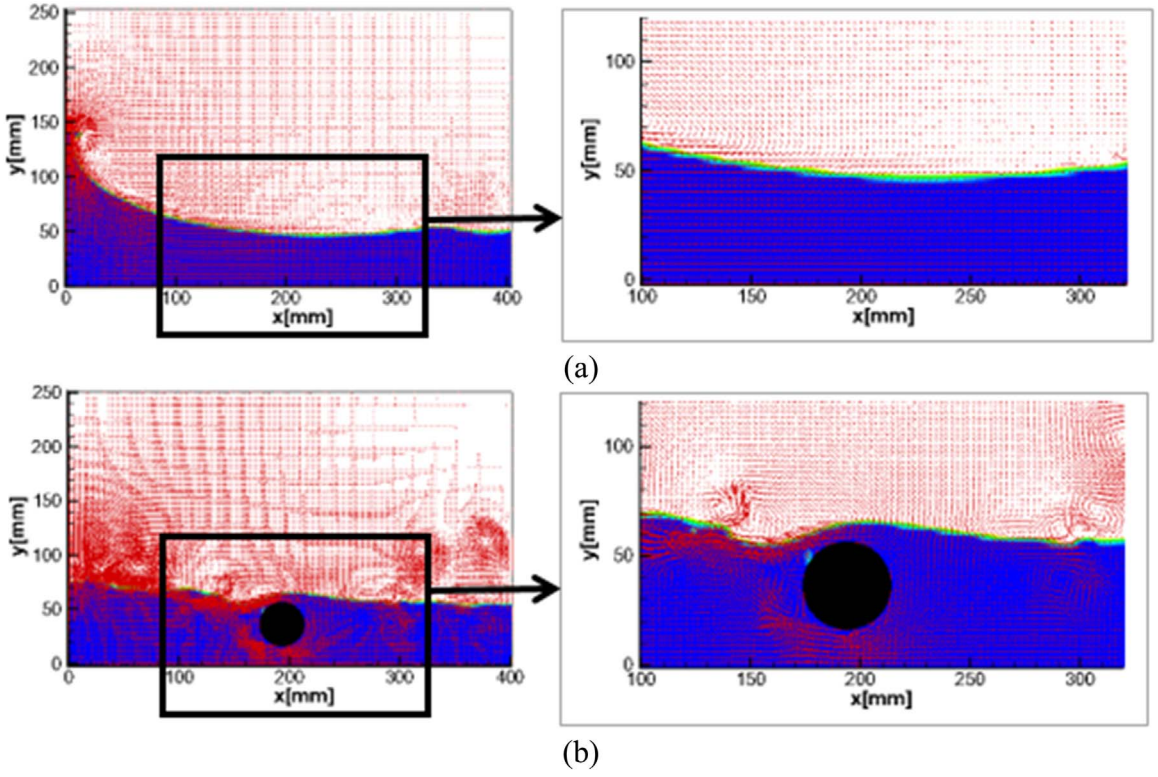

Fig. 14. Velocity field for liquid sloshing in a moving container undergoing the SOE in x-direction without (a) and with (b) the submerged cylinder at t=2.2 s (d6A10).

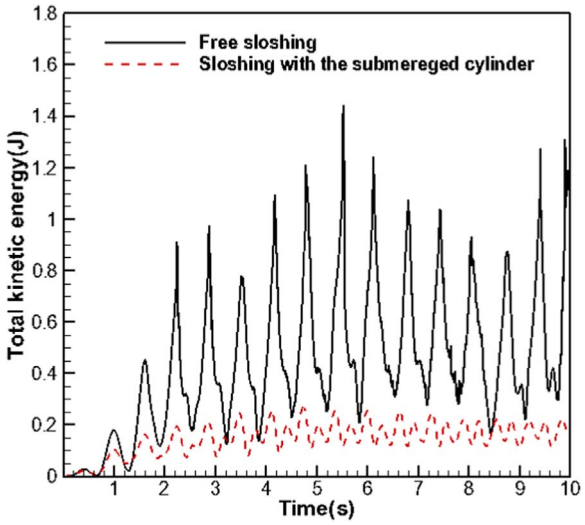

Fig. 15. Total kinetic energy of the liquid with and without the submerged cylinder versus time in a moving container undergoing the SOE in x-direction (d4A15).

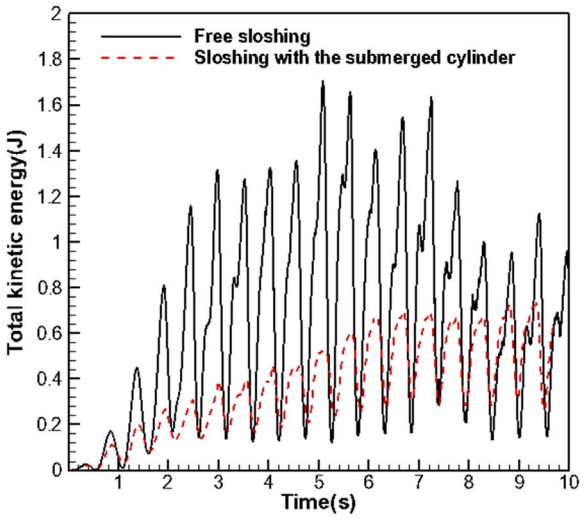

Fig. 16. Total kinetic energy of the liquid with and without the submerged cylinder versus time in a moving container undergoing the SOE in x-direction (d6A10).

where the mass of liquid within the cell and velocity in the body-fixed coordinate system (y-direction) are denoted by m_l and $\vec{v}$, respectively. Total kinetic energy of the liquid in the container can be obtained by summing up the kinetic energy of each cell occupied by the liquid. For a quantitative investigation of the effect of submerged cylinder, the total kinetic energy of the liquid within the container with free sloshing and with the submerged cylinder are depicted versus time in Fig. 9. The total kinetic energy of the fluid is maximum at initial times. The energy, however, decreases substantially as the time passes. The kinetic energy of the fluid with the submerged cylinder is about 0.1 J at t=3 s and it remains approximately constant until t=10 s. It should be explained that average of total kinetic energy is obtained by taking average of the total kinetic energy for each time step. The suppression rate of the kinetic energy is calculated as follows:

$$\text{Suppression rate of kinetic energy} = \frac{|\text{TKE}_{\text{ave,free}} - \text{TKE}_{\text{ave,sub}}|}{\text{TKE}_{\text{ave,free}}} \times 100 \tag{35}$$

where the average total kinetic energy for free sloshing and sloshing with the submerged cylinder are shown by $\text{TKE}_{\text{ave,free}}$ and $\text{TKE}_{\text{ave,sub}}$, respectively. It is estimated that total kinetic energy is decreased by nearly 26.58% using the submerged cylinder.

For the case of sloshing with submerged cylinder, the variations of power absorbed by dampers in x and y directions versus time are displayed in Fig. 10. The power absorbed by the oscillating cylinder in x-direction for a frictional damper is calculated as follows:

$$P_x = F_{d,x} \times U_s \tag{36}$$

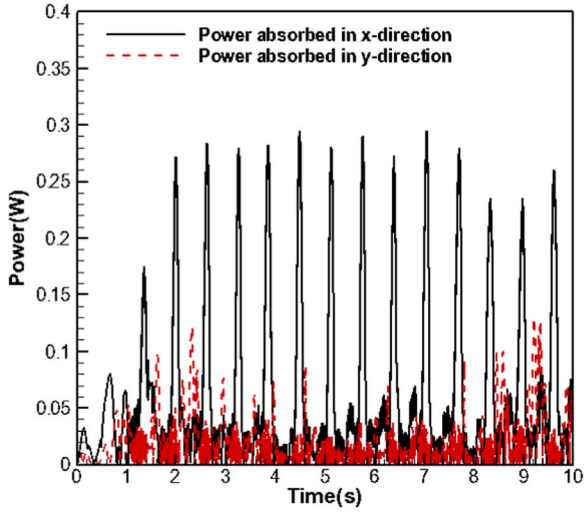

Fig. 17. Power absorbed by the damper undergoing the SOE in x and y directions versus time (d4A15).

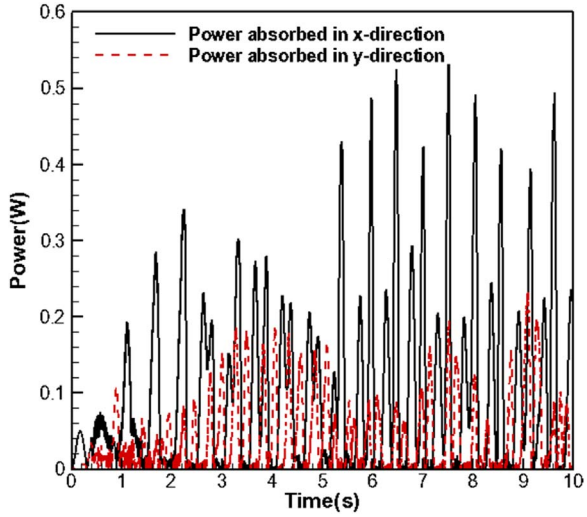

Fig. 18. Power absorbed by the damper undergoing the SOE in x and y directions versus time (d6A10).

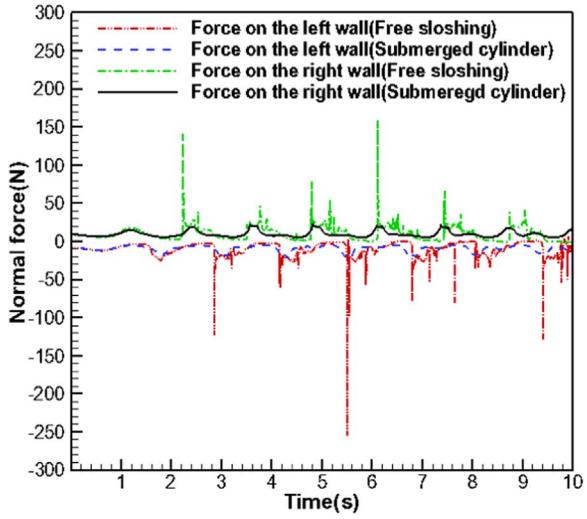

Fig. 19. The amount of normal forces exerted on the left and right walls subjected to the free sloshing and sloshing with the submerged cylinder (SOE and d4A15).

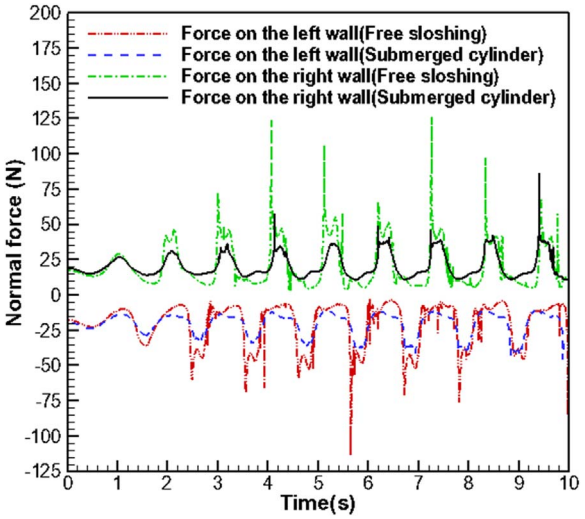

Fig. 20. The amount of normal forces exerted on the left and right walls subjected to the free sloshing and sloshing with the submerged cylinder (SOE and d6A10).

Table 5
Effects of the submerged cylinder on suppressing the kinetic energy of the liquid sloshing for various excitation amplitudes and water depths (SOE and γ=1).

		A=0.010 m γ=1	A=0.015 m γ=1	A=0.020 m γ=1
d=0.04 m	$U_{s,max}$(m/s)	0.0508	0.0682	0.088
	Re_{max}	1263.92	1696.84	2189.47
	$TKE_{ave,free}$(J)	0.3446	0.5666	0.7188
	$TKE_{ave,sub}$(J)	0.1074	0.1609	0.2188
	Rate of suppression(%)	68.83	71.60	69.56
d=0.06 m	$U_{s,max}$(m/s)	0.1232	0.1475	0.1900
	Re_{max}	4291.36	5137.79	6618.18
	$TKE_{ave,free}$(J)	0.7256	1.1909	1.5703
	$TKE_{ave,sub}$(J)	0.4287	0.4726	0.8255
	Rate of suppression(%)	40.92	60.32	47.43

Table 6
Effects of the submerged cylinder on suppressing the kinetic energy of the liquid sloshing for various frequency ratios (SOE and γ=1).

		A=0.015 m γ=0.9	A=0.015 m γ=1.0	A=0.015 m γ=1.1	A=0.015 m γ=1.2
d=0.04 m	$U_{s,max}$ (m/s)	0.0518	0.0682	0.1151	0.1634
	Re_{max}	1288.80	1696.84	2863.73	4065.45
	$TKE_{ave,free}$ (J)	0.2610	0.5666	0.7505	1.2167
	$TKE_{ave,sub}$ (J)	0.0968	0.1609	0.3289	0.5149
	Rate of suppression (%)	62.91	71.60	56.18	57.68

It is clear from Fig. 10 that the damping in x-direction plays a major role at the initial times of excitation for absorbing the power in comparison with that of the damping in y-direction. The amounts of Re and average of total kinetic energy for the CA are presented in Table 2. As shown in Table 2, the amount of Re falls within the subcritical range. Therefore, the regime is laminar (Koo et al., 2014).

The forces exerted on the left and right walls of the container experiencing free sloshing and sloshing with the submerged cylinder versus time are illustrated in Fig. 11. It is observed that the forces exerted on the left wall is greater than that of the right wall for both sloshing cases. The force on the left wall has an oscillatory behavior until t=10 s for the case of free sloshing. This oscillatory force may lead to fatigue and fracture of solid structures. The amplitude of these oscillatory forces for the left wall of container decreases over time for the free sloshing. As can be seen in Fig. 11, the value of the force on the left wall is approximately 70 N at

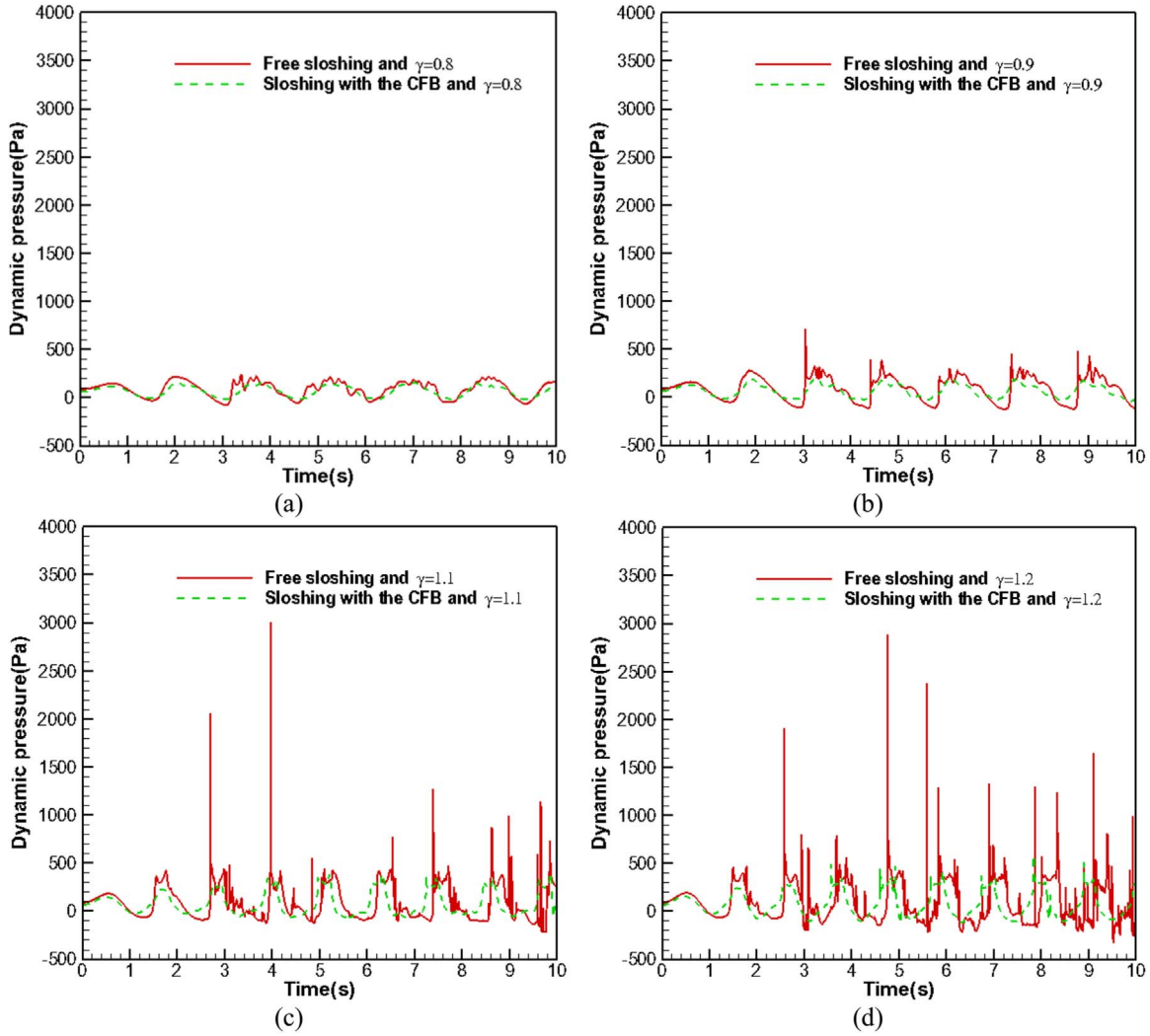

Fig. 21. Dynamic pressure of sloshing with the CFB compared to that of free sloshing at point P_4 for various frequency ratios: (a) γ=0.8 (b) γ=0.9 (c) γ=1.1 (d) γ=1.2.

Table 7
Effect of the cylinder diameter on suppressing the kinetic energy of the liquid sloshing undergoing the SOE (d4A15).

		D_x=0.02 D_y=0.02	D_x=0.02 D_y=0.025	D_x=0.02 D_y=0.03	D_x=0.025 D_y=0.02	D_x=0.025 D_y=0.025	D_x=0.025 D_y=0.03	D_x=0.03 D_y=0.02	D_x=0.03 D_y=0.025	D_x=0.03 D_y=0.03
SOE	$U_{s,max}$(m/s)	0.0703	0.0711	0.0696	0.0571	0.0682	0.0764	0.0582	0.0722	0.0818
	Re_{max}	1399.27	1415.19	1385.34	1420.67	1696.84	1900.86	1737.64	2155.63	2442.26
	$TKE_{ave,free}$(J)	0.5666								
	$TKE_{ave,sub}$(J)	0.2175	0.1578	0.0896	0.2124	0.1609	0.0873	0.228	0.1686	0.0959
	Rate of suppression (%)	61.61	72.15	84.19	62.51	71.60	84.59	59.76	70.24	83.07

t=5.0 s and it remains constant until t=10 s for sloshing with the submerged cylinder. Therefore, the submerged cylinder can eliminate the oscillatory forces exerted on the wall of container for the CA. The amounts of forces exerted on the right wall are approximately zero for both free sloshing and sloshing with the submerged cylinder after t=3.0 s.

3.3. Suppressing the kinetic energy of liquid sloshing undergoing the SOE

In this section, the effect of the submerged cylinder on mitigating the kinetic energy of the container undergoing the SOE is studied for different water depths and excitation amplitudes. Without any loss of generality, the case of a harmonic excitation is considered while the amplitude and frequency ratio are denoted by A and γ. Frequency ratio is defined as the ratio of excitation frequency (f) to fundamental sloshing frequency (f_w) of the liquid inside the rectangular tank:

$$\gamma = \frac{f}{f_w} \tag{37}$$

By using the linear wave theory, the fundamental sloshing frequency can be estimated as follows (Cavalagli et al., 2017):

$$f_w = \frac{1}{2\pi}\sqrt{\frac{\pi g}{L}\tanh\left(\frac{\pi d}{L}\right)} \tag{38}$$

where g stands for the gravity acceleration. In particular, water depths of 4 and 6 cm have been studied (indicated in the following d4 and d6), with amplitudes of 10 and 15 mm (indicated in the following as A10, A15). The amounts of the container size, the cylinder and other conditions are presented in Tables 3 and 4. The frequency ratio (γ) is

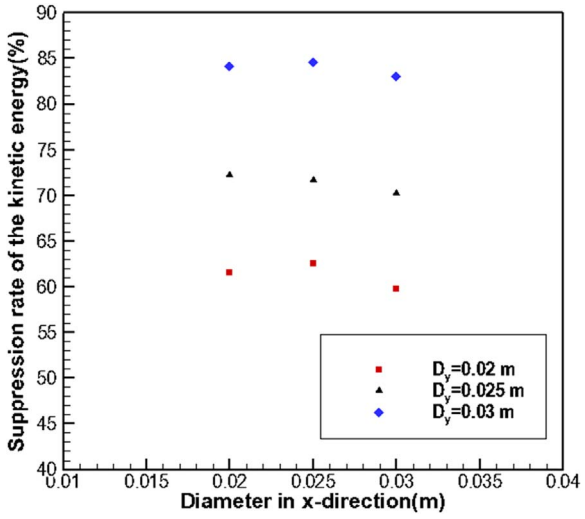

Fig. 22. Suppression rate of the kinetic energy of sloshing in a container subjected to the SOE using a submerged cylinder versus its diameter in x-direction (d4A15).

Table 8
Effects of the cylinder density on suppressing the kinetic energy of the liquid sloshing undergoing the SOE (d4A15).

		ρ_s (kg/m^3) =750	ρ_s (kg/m^3) =1000	ρ_s (kg/m^3) =1250
SOE	$U_{s,max}$(m/s)	0.074	0.0682	0.0675
	Re_{max}	1841.15	1696.84	1679.42
	$TKE_{ave,free}$(J)	0.5666		
	$TKE_{ave,sub}$(J)	0.1562	0.1609	0.1435
	Rate of suppression(%)	72.43	71.60	74.67

Table 9
Effects of projected length in x-direction on suppressing the kinetic energy of the liquid sloshing undergoing the SOE (L_y=0.02 and d4A15).

		β=45°	β=35°	β=25°
SOE	$U_{s,max}$(m/s)	0.0682	0.0618	0.0608
	Re_{max}	1696.84	1537.61	1512.73
	$TKE_{ave,free}$(J)	0.5666		
	$TKE_{ave,sub}$(J)	0.1609	0.1590	0.1563
	Rate of suppression(%)	71.60	71.94	72.41

Table 10
Effects of L_y on suppressing the kinetic energy of the liquid sloshing undergoing the SOE (d4A15).

		β=55°, L_y=0.0286	β=45°, L_y=0.02	β=35°, L_y=0.014
SOE	$U_{s,max}$(m/s)	0.0948	0.0682	0.0771
	Re_{max}	2358.66	1696.84	1918.28
	$TKE_{ave,free}$(J)	0.5666		
	$TKE_{ave,sub}$(J)	0.2059	0.1609	0.1387
	Rate of suppression(%)	63.66	71.60	75.52

set to be one to make the comparison with the experimental data easy.

The results of the container experiencing this oscillatory excitation with and without the submerged cylinder are shown in Figs. 12 and 13 (d4A15 and d6A10 cases). The violent sloshing waves generated by the SOE for both two cases are being suppressed well by the submerged cylinder since the water elevation at the left and right sides of the container are decreased as shown in the Figs. 12 and 13. It should be noted that the inertial forces dominate the capillary forces when the We number is greater than 80 (Malgarinos et al., 2014). The maximum We number for the case of the SOE(d4A15) is about 0.83. Therefore, the effects of capillary effects should be considered in the simulation. The Weber number (We) is calculated as follows:

$$We = \frac{\rho U_s^2(D)}{2\sigma} \tag{39}$$

where D stands for diameter of the cylinder.

To show the mechanism of the submerged cylinder in suppressing the kinetic energy of sloshing better, the velocity fields of the container with and without the submerged cylinder are illustrated in Fig. 14. The submerged cylinder suppresses the sloshing kinetic energy in two ways: absorbing the sloshing kinetic energy via frictional dampers and dissipating the kinetic energy by the recirculation zones induced via the submerged cylinder as shown in Fig. 14. Furthermore, the free surface deformation generated by the submerged cylinder and shear stress of walls play a very determinant role in dissipating the kinetic energy especially for shallow water depths. The liquid part of the container with free sloshing does not experience any recirculation zone while for the case of submerged cylinder, multi recirculation zones are generated within the liquid zone. More recirculation translates into more viscous dissipation within the liquid and, as a result, more mitigation of the liquid sloshing. This factor also decreases the water level at both left-hand and right-hand sides of the container as shown in Figs. 12 and 13. It should be noted that the kinetic energy of sloshing considers these two factors implicitly since the kinetic energy of sloshing is calculated for each cell occupied by liquid and the total amount of the kinetic energy is calculated by summing up these values for each time step.

Total kinetic energy of the fluid experiencing the SOE with and without the submerged cylinder for d4A15 and d6A10 cases are shown in Figs. 15 and 16. For both cases, the submerged cylinder can suppress the kinetic energy of sloshing well. It is estimated that the average kinetic energy of the fluid for d4A15 and d6A10 cases are decreased by 71.6% and 40.92% respectively by using the submerged cylinder. It is also found that the submerged cylinder has a greater impact in mitigating the average kinetic energy of the fluid with the SOE in comparison with that of the CA where the decrease of the kinetic energy was 26.58% (Fig. 9).

The rate of power absorbed by the submerged cylinder in x and y directions for d4A15 and d6A10 cases are illustrated in Figs. 17 and 18. As observed, the amount of power absorbed in x-direction is greater than that of the y-direction in most of the times for both cases considered. It is also found that the amount of power absorbed in y-direction for d6A10 is greater than that of d4A15.

The normal forces exerted on the left and right walls of the container with and without the submerged cylinder for d4A15 and d6A10 cases are depicted versus time in Figs. 19 and 20. It is clear that the maximum forces exerted on left and right walls for free sloshing of d4A15 is greater than that of d6A10. The amplitudes of the forces exerted on the left and right walls of the container are decreased considerably by using the submerged cylinder for d4A15 and d6A10. Although the cylinder suppresses the normal forces but they remain oscillatory due to the oscillatory nature of the excitation.

3.4. The effects of various parameters on the kinetic energy of the liquid undergoing an excitation with constant and variable acceleration

3.4.1. The amplitude and frequency of excitation

The effect of the submerged cylinder on reducing the kinetic energy of sloshing are investigated for three amplitudes of 10, 15, 20 mm and two water depths in Table 5 while the other parameters are the same as those presented in Tables 3 and 4. Regarding the free sloshing, the cases have been compared with experimental data to show that the flow regime is laminar (Figs. 12 and 13). For cases with the submerged cylinder, the maximum of Re falls within the subcritical range for all

cases considered (Koo et al., 2014) and the excitation with amplitudes of 15 mm has the highest suppression rate for both water depths investigated (Table 5). It should also be mentioned that the suppression rate of the cases with d=0.04 m are higher than those with d=0.06 m.

The capability of the submerged cylinder on suppressing the kinetic energy of the container undergoing various frequency ratios are studied in Table 6. As shown in Table 6, the suppression rate of the sloshing kinetic energy is the highest when the container is excited with the fundamental sloshing frequency. Dynamic pressure plays an important role for design of tanks since high dynamic pressure may cause fatigue damage to the tank wall. To understand the sloshing dynamics better, the effects of frequency ratio on the dynamic pressure at point P_4 for both free sloshing and sloshing with the CFB are investigated in Fig. 21. As shown in Fig. 21, dynamic pressure of sloshing with the CFB at point P_4 can be reduced significantly compared to that of free sloshing over a range of frequency close to the fundamental sloshing frequency. Furthermore, the amplitude of dynamic pressure for free sloshing and sloshing with the CFB depends highly on the excitation frequency ratio as shown in Fig. 21. It should be mentioned that the effect of submerged cylinder in decreasing the dynamic pressure is minor for frequencies lower than fundamental sloshing frequency while this effect becomes more significant as the frequency ratio increases.

3.4.2. The submerged cylinder geometry

In this section, the effect of the submerged cylinder geometry on suppressing the kinetic energy of the liquid sloshing for d4A15 is investigated. The comprehensive results of this investigation are given in Table 7. All the input data are the same as those presented in Table 3 except for the cylinder size; nine cases in total were considered (Table 7). As seen from Table 7, the rate of mitigation of kinetic energy increases as the cylinder diameter is increased for the SOE (cases with $D_x=D_y$). The effects of elliptical cylinders in reducing the kinetic energy are also investigated in Table 7. For the cases with the SOE, D_y plays a more prominent role in reducing the kinetic energy while the effects of D_x can be neglected as observed in Table 7 and Fig. 22.

3.4.3. The submerged cylinder density

The effects of three cylinder densities (750, 1000, 1250 kg/m^3) on mitigating the kinetic energy of the container undergoing the SOE are presented in Table 8. Based on Table 8, when the cylinder density is less than or equal to water density, the suppression rate of the kinetic energy of sloshing remains nearly constant for d4A15. Increasing the cylinder density, however, increases the suppression effects of the submerged cylinder on sloshing a little.

3.4.4. The spring-damper angle

To investigate the effects of spring-damper angle β (see Fig. 7) on suppression rate of the kinetic energy of sloshing, three values of 45°, 35°, 25° are considered for the SOE (d4A15) in Table 9 where L_y is assumed to remain at a constant value of 0.02 m. As stated before, the power is mostly absorbed in x-direction for the SOE; thus, the mitigation rate of the kinetic energy is increased as the spring-damper angle is reduced (i.e., cosβ is larger when β is smaller in the first quarter). The effects of projected length in y-direction (L_y) on mitigation rate of the kinetic energy are investigated in Table 10 while the projected length in x-direction remains constant (L_x=0.02 m). It is found that the suppression rate of the kinetic energy increases as the L_y is decreased.

4. Conclusions

In this paper, 2D sloshing of a container undergoing a constant (CA) and variable (SOE) acceleration excitation in presence of a submerged cylinder were studied numerically. The continuity and Navier-Stokes equations for the 2D incompressible fluid flow were solved along with an equation for the free surface advection. The developed numerical program was validated for both free sloshing and sloshing with the CFB. The results of simulations were in close agreement with both measurements and numerical results available in the literature. Next, the effects of the submerged cylinder shape, position, and density, and spring-damper angle, water depth, amplitude and frequencies of excitation on the suppression rate of the kinetic energy of sloshing were examined. The following conclusions were drawn briefly:

1. The average mitigation rate of the kinetic energy of sloshing for the CA, d4A15, and d6A10 (SOE) were 26.58%, 71.6%, and 40.92%, respectively.
2. The suppression rate of the sloshing kinetic energy for the SOE was the highest when the container was excited with the fundamental sloshing frequency.
3. For the SOE, cylinder diameter in y-direction had a more prominent role in reducing the sloshing kinetic energy while the effects of the cylinder diameter in x-direction could be neglected.
4. The suppression rate of total kinetic energy increased as the diameter of circular submerged cylinder was enlarged for the SOE (for cases with $D_x=D_y$).
5. The suppression rate of the kinetic energy of sloshing was almost the same when the cylinder density was equal or less than that of water for the SOE.
6. For the SOE motion, the mitigation rate of the kinetic energy was increased as the projected length in x-direction was enlarged because the power was mostly absorbed in x-direction.
7. It was found that the suppression rate of the kinetic energy increased as the L_y was decreased for the SOE.

Acknowledgements

The authors would like to acknowledge the high-performance computing (HPC) center of the Ferdowsi University of Mashhad.

References

Akyildiz, H., 2012. A numerical study of the effects of the vertical baffle on liquid sloshing in two-dimensional rectangular tank. J. Sound Vib. 331, 41–52.
Akyildiz, H., Unal, E., Aksoy, H., 2013. An experimental investigation of the effects of the ring baffles on liquid sloshing in a rigid cylindrical tank. Ocean Eng. 59, 190–197.
Akyildiz, H., Unal, E., 2005. Experimental investigation of pressure distribution on a rectangular tank due to the liquid sloshing. Ocean Eng. 32, 1503–1516.
Aleinov, I., Puckett, E.G., 1995. Computing surface tension with high-order kernels. In: Proceedings of the Sixth International Symposium on Computational Fluid dynamics. Lake Tahoe NV.
Anbarsooz, M., Passandideh-Fard, M., Moghiman, M., 2014. Numerical simulation of a submerged cylindrical wave energy converter. Renew. Energy 64, 132–143.
Brackbill, J.U., Kothe, D.B., Zemach, C., 1992. A continuum method for modeling surface tension. J. Comput. Phys. 100, 335–354.
Budiansky, B., 1960. Sloshing of liquids in circular canals and spherical tanks. J. Aerosp. Sci. Technol. 27, 161–173.
Cavalagli, N., Biscarini, C., Facci, A.L., Ubertini, F., Ubertini, S., 2017. Experimental and numerical analysis of energy dissipation in a sloshing absorber. J. Fluids Struct. 68, 466–481.
Celebi, M.S., Akyildiz, H., 2002. Nonlinear modeling of liquid sloshing in a moving rectangular tank. Ocean Eng. 29, 1527–1553.
Chiba, M., 1995. Free vibration of a partially liquid-filled and partially submerged in a liquid. J. Acoust. Soc. Am. 97, 2238–2248.
Dutta, S., Laha, M.K., 2000. Analysis of the small amplitude sloshing of a liquid in a rigid container of arbitrary shape using a low-order boundary element method. Int. J. Numer. Methods Eng. 47, 1633–1648.
Ebrahimian, M., Noorian, M.A., Haddadpour, H., 2013. A successive boundary element model for investigation of sloshing frequencies in axisymmetric multi baffled containers. Eng. Anal. Bound. Elem. 37, 383–392.
Elahi, R., Passandideh-Fard, M., Javanshir, A., 2015. Simulation of liquid sloshing in 2D containers using the volume of fluid method. Ocean Eng. 96, 226–244.
Faltinsen, O.M., Firoozkoohi, R., Timokha, A.N., 2011. Analytical modeling of liquid sloshing in two-dimensional rectangular tank with a slat screen. J. Eng. Math. 9, 93–109.
Faltinsen, O.M., Timokha, A.N., 2009. Sloshing. Cambridge University Press, Cambridge.
Glowinski, R., Pan, T.W., Hesla, T.I., Joseph, D.D., 1999. A distributed Lagrange multiplier/fictitious domain method for particulate flows. Int. J. Multiph. Flow. 25, 755–794.

Glowinski, R., Pan, T.W., Hesla, T.I., Joseph, D.D., Periaux, J., 2001. A fictitious domain approach to the direct numerical simulation of incompressible viscous flow past moving rigid bodies: application to particulate flow. J. Comput. Phys. 169, 363–426.
Goudarzi, M.A., Sabbagh-Yazdi, S.R., 2012. Analytical and experimental evaluation on the effectiveness of upper mounted baffles with respect to commonly used baffles. Ocean Eng. 42, 205–217.
Harlow, F.H., Amsden, A.A., 1971. A LASL monograph (Mathematical solutions for problems in fluid dynamics) LA 4700 Los Alomas National Laboratory.
Hasheminejad, S.M., Mohammadi, M.M., 2011. Effect of anti-slosh baffles on free liquid oscillations in partially filled horizontal circular tanks. Ocean Eng. 38, 49–62.
Heikkinen, H., Lampinen, M.J., Boling, J., 2013. Analytical study of the interaction between waves and cylindrical wave energy converters oscillating in two modes. Renew. Energy 50, 150–160.
Hwang, S.C., Park, J.C., Gotoh, H., Khayyer, A., Kang, K.J., 2016. Numerical simulations of sloshing flows with elastic baffles by using a particle-based fluid-structure interaction analysis method. Ocean Eng. 118, 227–241.
Ibrahim, R.A., 2005. Liquid Sloshing Dynamics. Cambridge University Press, Cambridge.
Iranmanesh, A., Passandideh-Fard, M., 2017. A three-dimensional numerical approach on water entry of a horizontal circular cylinder using the volume of fluid technique. Ocean Eng. 130, 557–566.
Isaacson, M., Premasiri, S., 2001. Hydrodynamic damping due to baffles in a rectangular tank. Can. J. Civ. Eng. 28, 608–616.
Koo, B., Yang, J., Yeon, S.M., Stern, F., 2014. Reynolds and froude number effect on the flow past an interface-piercing circular cylinder. Int. J. Nav. Archit. Ocean Eng. 6, 529–561.
Kershaw, D.S., 1978. The incomplete Cholesky–conjugate gradient method for the iterative solution of systems of linear equations. J. Comput. Phys. 26, 43–65.
Koh, C.G., Luo, M., Gao, M., Bai, W., 2013. Modelling of liquid sloshing with constrained floating baffle. Comput. Struct. 122, 270–279.
Li, H.T., Li, J., Zong, Z., Chen, Z., 2014a. Numerical studies on sloshing in rectangular tanks using a tree-based adaptive solver and experimental validation. Ocean Eng. 82, 20–31.
Li, J.G., Hamamoto, Y., Liu, Y., Zhang, X., 2014b. Sloshing impact simulation with material point method and its experimental validations. Comput. Fluids 103, 86–99.
Liu, D., Lin, P., 2008. A numerical study of three-dimensional liquid sloshing in tanks. J. Comput. Phys. 227, 3921–3939.
Liu, D., Lin, P., 2009. Three-dimensional liquid sloshing in a tank with baffles. Ocean Eng. 36, 202–212.
Luo, M., Koh, C.G., Bai, W., 2016. A three-dimensional particle method for violent sloshing under regular and irregular excitations. Ocean Eng. 120, 52–63.
Maleki, A., Ziyaeifar, M., 2008. Sloshing damping in cylindrical liquid storage tanks with baffles. J. Sound Vib. 311, 372–385.
Malgarinos, I., Nikolopoulos, N., Marengo, M., Antonini, C., Gavaises, M., 2014. VOF simulations of the contact angle dynamics during the drop spreading: standard models and a new wetting force model. Adv. Colloid Interface Sci. 212, 1–20.
Malvandi, A., Ghasemi, A., Nikbakhti, R., Ghasemi, A., Hedayati, F., 2016. Modeling and parallel computation of the non-linear interaction of rigid bodies with incompressible multi-phase flow. Comput. Math. Appl. 72, 1055–1065.
Mirzaii, I., Passandideh-fard, M., 2012. Modelling free surface flows in presence of an arbitrary moving object. Int. J. Multiph. Flow. 39, 216–226.
Panigrahy, P.K., 2006. Development of a Test Setup to Study the Sloshing Behavior of Liquids in Baffled Tanks (M.Tech. thesis). Department of Mechanical Engineering IIT Guwahati, India.
Patankar, N.A., 2001. A formulation for fast computations of rigid particulate flows. In: Center for Turbulence Research, editor Annual research briefs Evanston Northwestern University.
Patankar, N.A., Singh, P., Joseph, D.D., Glowinski, R., Pan, T.W., 2000. A new formulation of the distributed Lagrange multiplier/fictitious domain method for particulate flows. Int. J. Multiph. Flow. 26, 1509–1524.
Sharma, N., Patankar, N.A., 2005. A fast computation technique for the direct numerical simulation of rigid particulate flows. J. Comput. Phys. 205, 439–457.
Veldman, A.E.P., Gerrits, J., Luppes, R., Helder, J.A., Vreeburg, J.P.B., 2007. The numerical simulation of liquid sloshing on board spacecraft. J. Comput. Phys. 224, 82–99.
Wang, W., Guo, Z., Peng, Y., Zhang, Q., 2016a. A numerical study of the effects of the T-shaped baffles on liquid sloshing in horizontal elliptical tanks. Ocean Eng. 111, 543–568.
Wang, Z., Zou, L., Zong, Z., 2016b. Three dimensional sloshing of stratified liquid in a cylindrical tank. Ocean Eng. 119, 58–66.
Wu, C.H., Faltinsen, O.M., Chen, B.F., 2012. Numerical study of sloshing liquid in tanks with baffles by time-independent finite difference and fictitious cell method. Comput. Fluids 63, 9–26.
Wu, N.J., Hsiao, S.C., Wu, H.L., 2016. Mesh-free simulation of liquid sloshing subjected to harmonic excitations. Eng. Anal. Bound. Elem. 64, 90–100.
Xue, M.-A., Lin, P., 2011. Numerical study of ring baffle effects on reducing violent liquid sloshing. Comput. Fluids 52, 116–129.
Xue, M.-A., Lin, P., Zheng, J., Ma, Y., Yuan, X., Nguyen, V.-T., 2013. Effects of perforated baffle on reducing sloshing in rectangular tank: experimental and numerical study. China Ocean Eng. 27, 615–628.
Youngs, D.L., 1984. An Interface Tracking Method for a 3D Eulerian Hydrodynamics Code. Technical report 44/92/35 AWRE.
Zhang, C., 2015a. Analysis of liquid sloshing in LNG carrier with wedge-shaped tanks. Ocean Eng. 105, 304–317.
Zhang, C., 2015b. Application of an improved semi-Lagrangian procedure to fully-nonlinear simulation of sloshing in non-wall-sided tanks. Appl. Ocean Res. 51, 74–92.
Zhang, C., Li, Y., Meng, Q., 2015. Fully nonlinear analysis of second-order sloshing resonance in a three-dimensional tank. Comput. Fluids 116, 88–104.